João Carlos Galveias Lopes

Licenciado em Ciências de Engenharia Mecânica

Feasibility of the milling process on HSLA parts produced with Wire and Arc Additive Manufacturing

Dissertação para obtenção do Grau de Mestre em Engenharia de Mecânica

Orientadora: Doutora Carla Maria Moreira Machado, Professora Auxiliar, Faculdade de Ciências e Tecnologia da Universidade Nova de Lisboa

Coorientador: Doutor João Pedro de Sousa Oliveira, Professor Auxiliar, Faculdade de Ciências e Tecnologia da Universidade Nova de Lisboa

Júri:

Presidente: Doutor Telmo Jorge Gomes dos Santos

Arguente: Doutor Bruno Alexandre Rodrigues Simões Soares,

Vogal: Doutora Carla Maria Moreira Machado

FACULDADE DE CIÊNCIAS E TECNOLOGIA
UNIVERSIDADE NOVA DE LISBOA

Setembro, 2019

Feasibility of the milling process on HSLA parts produced with Wire and arc additive manufacturing

To my family

Acknowledgments

First, I would like to thank my supervisor, Professor Carla Machado, for her knowledge, resilience, patience and mostly for the incentive that she provided during the analysis experimental results. I will never forget the day she told me to “think outside the box” and I am honoured to have had the possibility to learn from her.

Secondly, I must express my gratitude towards my co-supervisor, Professor João Oliveira, for his defiant spirit and for never allowing the work to become dull. I am certain that he is one of the most inspiring persons I have ever known.

For their help, friendship, knowledge and support, my sincere thanks to Valdemar and Tiago, the two solid foundations for the beginning of the experimental work.

My gratitude must also be expressed towards Rui Maltez and Antonio Maltez, for their knowledge, advice and for the numerous hours spent on machining the samples.

I am also grateful to Professor Telmo Santos for his ideas and for the scanner utilized in the waviness measurements.

To Mr. António Campos and Mr. Paulo Magalhães, for their encouragement, friendship and for always being ready to help.

My sincere thanks also go to Patrick, Professor Catarina Vidal, Francisco and Professor Pamies Teixeira for their opinions and knowledge.

An important mention must also be made towards Professor Alberto Martinho for lending the torque wrench utilized for fixing the samples during the milling operations.

To my friends and colleagues to for easing the mood in the laboratory, especially Grigore, Vanda, Daniel, Stefan, José, Guilherme, Flávio, Carlos and André. My thanks also go to Tiago Pedro, Diogo Machado, Bruno, Tiago Pratas and Filipa for the several laughs and incentive provided during the experimental work.

Finally, to my family for their constant comprehension, encouragement and for relieving me from my responsibilities during the writing of this document.

Resumo

Atualmente, o fabrico aditivo é considerado como um grande impulsionador de uma nova revolução industrial. Os mais recentes avanços nesta área evidenciam que *Wire and Arc Additive Manufacturing* (*WAAM*) demonstra potencial para se tornar um processo relevante para a produção de componentes metálicos, em larga escala. Neste estudo, foi reconhecida a necessidade de pós-processamento de tais componentes, o que levou à caracterização do processo de fresagem em relação às propriedades características a estas peças.

Primeiramente, as estruturas necessárias para as operações de fresagem foram fabricadas e caracterizadas usando duas entregas térmicas diferentes. De seguida, foi aplicada uma estratégia de fresagem que considera as características das peças *WAAM*, onde os parâmetros de processo e as ferramentas utilizadas foram escolhidos com base nas informações fornecidas pelo fabricante da ferramenta.

Concluiu-se que as propriedades inerentes aos componentes produzidos por *WAAM* influenciam o processo de fresagem e que a qualidade das superfícies melhora significativamente com o aumento da velocidade de corte e com a diminuição do avanço por dente. No entanto, é necessária mais investigação para a caracterização do processo de fresagem em componentes produzidos por *WAAM* devido aos mecanismos de desgaste das ferramentas associados ao material das peças maquinadas.

Palavras-chave:

Fabrico aditivo, Aresta postiça de corte, Aço de alta resistência e baixa liga, pós-processamento, fresagem de rasgos, WAAM

Abstract

Nowadays, additive manufacturing is considered an important propeller for a new industrial revolution. The recent advances in this manufacturing approach show that Wire and arc additive manufacturing (WAAM) has the potential to become a relevant method for the production of metallic components on a large scale. In this study, the need for the post-processing of these parts was recognized, which led to the characterization of the milling process regarding the several properties inherent to these parts.

The thin-walled structures required for the milling operations were manufactured using two different heat inputs. Then, a milling strategy that has in consideration the characteristics of such components was applied, where the process parameters and the tools utilized during the experiments were chosen based on the information provided by the tool manufacturer.

The results show that the properties inherent to the components manufactured via WAAM have influence in the milling process and that the quality of the surfaces improves with the increase of cutting speeds and with the decrease of feed per tooth. Nevertheless, more investigation is required to accurately study the milling process on WAAM parts due to the tool wear mechanisms associated with the workpiece material

.

***Keywords**:*

Additive manufacturing, build-up edge, HSLA steel, post-processing, slot milling, WAAM

Contents

List of figures

List of tables

Nomenclature and symbols

AM	Additive manufacturing
a_e	Radial depth of cut
a_p	Axial depth of cut
BUE	Build-up edge
CLAD	Laser cladding
DAQ	Data acquisition
DED	Directed energy deposition
DLMD	Direct laser metal deposition
F	Feed rate
F_c	Cutting force on the oblique cutting model
f_z	Feed per tooth
GMAW	Gas Metal Arc Welding
GTAW	Gas Tungsten Arc Welding
h	Uncut chip thickness
h_c	Chip thickness
i	Obliquity angle
HSLA	High strength low alloy steel
lr	Sampling length
PAW	Plasma arc welding
PBF	Powder bed fusion
Ra	Arithmetical mean deviation of the accessed profile
R	Resultant cutting force on the oblique cutting model
Rz	Maximum height of the profile
S	Spindle speed
v_c	Cutting speed
WAAM	Wire and Arc Additive Manufacturing
Z	Number of teeth
Z(x)	Height of the profile
α	Rake angle
α_n	Rake angle in the plane normal to the cutting edge
η	Chip flow angle
ζ	Chip compression ratio
φ	Instantaneous immersion angle

1

Introduction

1.1 Motivations and Objective

Based on the concept of creating an object in a layer by layer fashion, additive manufacturing (AM) has been increasingly growing for the past decades. In fact, the versatile and cost-efficient approach for the production of components makes it a considerable motivator for a new industrial era, as it is proven by the wide the range of materials that can be subjected to these technologies.

Wire and Arc Additive Manufacturing (WAAM) is a known AM technique that allows for the rapid manufacturing of metallic parts. However, some challenges regarding the mechanical behaviour and the surface quality represent a major concern on the manufactured parts. Thus, the further development of this technology relies on post-processing operations made in order to mitigate the superficial characteristics inherent to the process.

Moreover, from a hybrid manufacturing perspective, the combination of the AM advantages, such as freedom of design and reduction of material waste and costs, with the benefits obtainable through known subtractive techniques, for example milling or turning, offers a path to efficiently develop ready-to-use components, by reducing the manufacturing process time and costs [1]. Therefore, a research on the cutting mechanism outcomes and parameters is required to improve the WAAM process towards the increase of the industrial manufacturing efficiency.

In consideration of the aforementioned, the main objective of this thesis is to study the interaction between the milling process and the WAAM technology, through the investigation of the characteristics of the produced parts on the outcomes of the milling process.

1.2 Document structure

This thesis is organized in five chapters:

Chapter 1: the motivations and the objectives of this thesis are presented.

Chapter 2: highlights the state of the art on the additive manufacturing of metals, namely WAAM, provides an overview of the ongoing scientific developments on the machining process of additively manufactured components and gives a brief introduction of the milling process.

Chapter 3: the experimental procedure, the materials and the characterization techniques utilized for the analysis of the experiments are described.

Chapter 4: presents and discusses the results obtained through the experimental work.

Chapter 5: the main conclusions and proposals for future work are summarized.

2

Literature Review

2.1 Additive manufacturing of metallic components

The recent advances in additive manufacturing of metals made towards the increased freedom of design and focused on the reduction of production costs and material wastage, have been growing in numerous industrial sectors, predominantly aerospace, defence, biomedical and automotive. Currently, the most common methods for this manufacturing approach are based in Powder Bed Fusion (PBF) and Directed Energy Deposition (DED), although other procedures have already been developed, as in the case of cold spraying and friction stir deposition [2].

According to the standard ISO/ASTM 52900:2015 [3], PBF is a category of processes in which thermal energy selectively fuses regions of a powder bed; examples of these processes are Selective Laser Melting, Selective Laser Sintering and Electron Beam Melting.

The DED processes are characterized by the simultaneous fusion and deposition of the feedstock material, through the application of thermal energy. A further description of the processes belonging to this category resides in the type of primary heat source: laser, electron beam or plasma arc, and in the type of feedstock material in use: wire or powder.

The main differences between PBF and DED processes can be established in terms of the finished parts quality, manufacturing costs and speed and equipment complexity. In PBF, the surface quality of the printed parts depends mainly on the size of the powder grains and, while limiting the dimensions of the components, the powder bed also acts as an integrated support structure. Additionally, the manufacturing process is relatively slow when compared with other processes, such as those using arc-based heat sources.

At the same time, the DED approaches are able to deliver reduced manufacturing time and costs, presenting some limitations regarding the dimensional accuracy and mechanical performance of the manufactured parts [2,4].

2.2 Wire and Arc Additive Manufacturing

As a DED process, WAAM has the capacity to manufacture large components with a high deposition rate, low equipment cost and consequent lower environmental impact. The ability to use wire as feedstock increases the efficiency of the process when compared to powder-based techniques by avoiding the necessity for constrained build volumes and powder recycling. Moreover, from a heat source point of view, an electric arc is more advantageous since does not require a vacuum environment and, in contrast with laser-based methods, it enables a higher energy efficiency when using reflective metal alloys as feedstock material.

Based on the approach used to create the electric arc, WAAM can be achieved through three different techniques, namely gas metal arc welding (GMAW), gas tungsten arc welding (GTAW) and plasma and arc welding (PAW). By comparison, GTAW and PAW are more stable processes than GMAW, having fewer problems of sputtering, weld fumes, excessive heating and other concerns on the manufactured parts integrity. Nevertheless, in these two technologies, the wire is not fed coaxially, which can lead to problems in achieving consistent metal deposition. Additionally, the deposition rate of GMAW is 2-3 times higher than that of GTAW and PAW technologies, ranging from 2- 3 kg/hour to 6-8 kg/hour [5,6].

As a function of heat input, the metal deposition affects the final quality and mechanical performance of the manufactured parts. For instances, with a higher heat input, a larger volume of material can be deposited, although with less accuracy in what concerns the quality of the surfaces. This amount of energy introduced during the process is influenced by current intensity, voltage and travel speed. Other parameters, such as shielding gas type and flow rate, contact-tip-to-work distance, wire feed speed, deposition strategy and torch angle also influence the WAAM process [7]. In this context, the solidification and heat dissipation processes are the main cause for the characteristic grain structure and crystallographic texture, that in turn promote anisotropy on the manufactured part. During the deposition of material, the nucleation and grain growth mechanisms mainly depend on the chemical composition of the previously deposited layer/substrate. However, in the cases where a similar chemical composition is employed, the nucleation of a new phase with a different crystal structure is not required to allow the epitaxial growth of the grains, as long as the temperature drops below the melting point. This absence of nucleation mechanisms induces the formation of large columnar grains, that result from the competitive growth that occurs between dendrites with various crystallographic orientations, where the predominant orientation corresponds to the maximum

thermal gradient. Nevertheless, this aligned microstructure is unfavourable, since it influences the mechanical behaviour of the part depending on the loading direction.

Additionally, the heat dissipation rate and the thermal cycling also have an important role in the material properties and residual stresses, since it affects the size of the melt pool and may result in higher interlayer temperatures, which leads to localized variations on the microstructure in the regions thermally affected by the melt pool and for the development of dissimilar microstructures in different areas of the manufactured part [5,8].

2.2.1 Challenges associated with WAAM components

Although all the advantages that WAAM can exhibit as a metallic additive manufacturing method there are still some challenges that need to be surpassed. As established in the literature [5–7], the main defects on the deposited parts are poor surface quality, porosity, deformation, residual stresses and cracking. Nevertheless, in steels, the most problematic are the surface quality and the residual stresses. Also, the magnitude of each of these defects depends on the process parameters selection and on the type of feedstock material in use.

Regarding the quality of the as-built surfaces, WAAM components exhibit problems associated to poor dimensional accuracy, to the uneven surfaces caused by the characteristic waviness of the layer by layer approach and to the spatter characteristic from welding-based methods, as it can be observed in Figure 2.1. On this subject, Xiong et al. [9], researched the influence of the process parameters on the surface of thin-walled structures manufactured with H08Mn2Si wire electrode, using WAAM. It was found that the quality of the surfaces benefited from the decrease of the interlayer temperature and that the surface profile improved with lower values of wire feed speed, while maintaining the ratio between this parameter and the travel speed constant.

Figure 2.1 Surface quality of as-built WAAM parts (From [10])

Still, despite the progresses made towards the improvement of the quality of WAAM parts, these still require to be complemented with post-processing, through machining operations, to surpass the aesthetical and dimensional limitations associated with these components.

Another problem associated with the WAAM parts are the residual stresses developed by the thermal contraction, caused by the multiple heating and cooling cycles that the deposited material undergoes in each deposition. In WAAM, these can reach values up to the ultimate tensile strength, being often associated with the occurrence of deformation and cracking, influencing the fatigue performance and corrosion resistance.

Although being a subject that still requires intensive research, a comparison on the residual stresses and microstructure on Ti-6Al-4V produced by WAAM and CLAD was presented by Szost et al. [11]. It was concluded that the distribution of the residual stresses is uneven throughout the thin-walled structures. The maximum magnitude of these residual stresses occurred in the longitudinal direction, where more material exists to constrain the manufactured part. The microstructure showed that the CLAD samples presented narrow wavy columnar grains, while in the WAAM samples large columnar grains were observed. Similar conclusions on the residual stress distribution were also observed in aluminium and steel alloys [12,13].

Furthermore, other methods for improving WAAM have already been set in order. Such is the case of the application of double-wire feed processing where an increased deposition rate and superior mechanical properties, microstructure and bead appearance can be achieved [14–16]. Also, through the hybrid manufacturing techniques, the enhancement of the process with the potential of monitoring the manufacturing process can offer a more reliable approach and relatively faster way to achieve the expected results, as Lopez et al. [17] verified while studying the suitability of existing non-destructive testing techniques for the inspection of WAAM parts.

2.3 Post-processing of additive manufacturing components

As the progress on additive manufacturing technologies increases, so does the necessity to make them viable in achieving the requirements imposed by the industrial world. Hence, considering the different physical principles and phenomena associated with the additive manufacturing processes, in this section it is intended to survey the literature about the post-processing of AM components and to understand the ongoing developments regarding the HSLA steels. Later, more emphasis is given to the milling process with the purpose of establishing the current state-of-the-art on the subject.

In the literature, it can be noted that the post-processing of AM components is mostly focused on additive manufacturing technologies based in PBF, nevertheless, some studies on the post-processing of DED manufactured parts can also be found. For this reason, in Table 2.1 and Table 2.2 several research highlights regarding the overall progress in this subject are summarized.

Table 2.1 Studies on the superficial post-processing of additive manufacturing components

Reference	AM category	Observations
Du et al. [18]	**PBF** (Laser based)	Milling operations were performed on 18Ni-300 maraging steel, regarding of an additive/subtractive hybrid manufacturing approach that combines PBF with milling. The AM samples exhibited higher cutting forces when compared with wrought ones.
Sartori et al. [19]	**PBF** (Electron Beam and Laser based)	Tuning operations were executed on Ti-6Al-4V parts, in order to study the tool wear mechanisms, relating dry and cryogenic turning with the manufacturing technique and with the material properties. The most important effect of the cryogenic cooling was the reduction of the cutting temperature, which prevented the mechanisms responsible for the crater wear formation on the tool rake face.
Bordin et al. [20]	**PBF** (Electron Beam based)	The turning process was researched on Ti-6Al-4V, while focusing on dry and cryogenic machining as eco-friendly strategies. It was shown that the cryogenic cooling strategy exhibited better results on the machined surfaces.
Groove et al. [21]	**PBF** (Laser based)	Milling operations were executed in Ti-5Al-5V-5Mo-3Cr alloy. This research focused on a comparison of the cutting forces, chip morphology, tool wear, surface quality and residual stresses on the samples. The results showed that the machinability of the conventionally manufactured alloys is distinct from that the additively manufactured parts, which was verified through the differences in the chip formation mechanisms.
Struzikiewicz et al. [22]	**PBF** (Laser based)	Turning operations were performed on an AlSi10Mg alloy. The resultant machined surfaces of the AM parts exhibited several cracks and voids, caused by the porosity of the inherent to the PBF processes. Lower cutting forces were achieved on the AM samples when compared with cast ones.
Fortunato et al. [23]	**PBF** (Laser based)	The milling process was studied in additively manufactured 18Ni-300 maraging steel. The influence of the process parameters on heat-treated and as-built samples was investigated on the surface roughness, hardness, microstructure, cutting forces, and tool wear. It was found that heat-treated samples showed better surface roughness and decreased tool wear.
Rotella et al. [24]	**PBF** (Electron Beam and Laser based)	Turning operations were conducted on Ti-6Al-4V. The results showed that different manufacturing techniques lead to different outcomes on the microstructure and topography of the machined surfaces, even when the components have an identical chemical composition. An important conclusion was that the cutting process parameters are so far optimized for conventional manufacturing techniques.
Oyelola et al. [25]	**DED** (Laser based)	Turning operations were performed on Ti-6Al-4V. Two cutting strategies were employed, one for the removal of the outer-layer and the other for the cutting parameters study on the bulk material. The AM samples exhibited higher machining forces when compared to wrought ones, also an annealing heat treatment reduced the cutting forces by 40%, at low cutting speeds.

Table 2.2 Additional studies on the superficial post-processing of additive manufacturing components

Reference	AM category	Observations
Brushi et al. [26]	**PBF** (Electron Beam based)	The turning process was studied on Ti-6Al-4V. The effects of the machining parameters and of the cooling strategy were studied, revealing that cryogenic cooling offers a significant improvement on the tool wear performance. The results showed that this cooling strategy offers a reduction on post-processing cleaning operations making it a competitive approach for the biomedical industry.
Calleja et al. [27]	**DED** (Laser based)	Milling and turning operations were performed on Inconel 718. Both additive manufactured samples, with and without heat treatment, exhibited higher surface roughness than the conventionally manufactured material. The cutting forces on the as-deposited samples were lower than that heat-treated samples.
Gong and Li [28]	**DED** (Laser based)	Milling operations were conducted on 316 L stainless steel parts. It was observed three different stages in the tool life and in the surface quality behaviour. Additionally, it was asserted that down milling results on a superior quality of the surface.
Bai et al. [29]	**DED** (Laser based)	The milling process was carried on ASTM A131 steel. The surface roughness was significantly improved by the post-processing. Different magnitudes for the cutting forces were observed when machining different areas of the components.

The integration of the traditional subtractive technologies with WAAM can also offer significant material and energy savings when compared to pure subtractive approaches. Already in the industry, several machine tool manufacturers have started to develop hybrid solutions that are capable of conjoining the additive and the subtractive technologies, aiming for the production of ready-to-use components and accelerating the progress towards a new industrial revolution. Some examples of these manufacturers are DMG Mori [30], Mazak [31] and DMS [32]. Additionally, solutions to hybridise existing CNC platforms are also available, as in the case of AMBIT™ developed by Hybrid Manufacturing Technologies [33].

On the subject of HSLA steels, these are characterized by their high strength, superior weldability, and exceptional ductility and impact toughness, which in turn, are influenced by the microstructure resultant from the manufacturing processes and chemical composition, composed of small amounts of alloying elements [34]. Nowadays, this category of steels is widely used in several industrial sectors [35–37], due to the ability to produce smaller components with superior mechanical properties. It is, therefore, these characteristics that make the HSLA steels attractive for research under the additive manufacturing approach.

Rodrigues et al. [10], investigated the influence of the thermal cycles on thin-walled structures manufactured through WAAM, by comparing a high heat input with a low heat input. The results showed that the different cooling rates developed during manufacturing influence the microhardness, microstructure and mechanical properties, as well as the superficial waviness and width of both samples.

Wang et al. [38] also studied HSLA steels produced through the DLMD process, concluding that the high cooling rates achievable through this laser-based technique allow for a fast and reliable method to manufacture components with a refined microstructure and good mechanical properties.

Nevertheless, the current status of the literature lacks knowledge concerning the machinability of components produced via Wire and arc additive manufacturing.

2.3.1 Post-processing through milling operations

Among the diverse methods that can be utilized for the post-processing of additive manufacturing components, milling is a conventional technique that is well established in the modern industry. As a result from the stress-induced plastic deformation and removal of small fragments of material, it provides a reliable solution to manufacture ready-to-use parts on a large scale.

Currently, several developments on the milling process consist on the accurate prediction of the different responses of the process. These provide the means to accurately model and study the physical processes that occur during machining of a determined material. Shi et al. [39] developed a model that allows for the evaluation of the total energy consumption on the overall milling process, considering the energy consumption required when the machine tool is idle and the different power requirements to cut different materials. Karaguzel and Budak [40], modelled the temperature developed during the milling process, relating the tool temperature with the radial depth of cut, comprising the striking and sliding contact of the rake face of the tool and a 3D transient heat conduction model.

Milling is characterized by the intermittent cutting action developed by the teeth entering and leaving the cut, where the contact period of the cutting edge with the workpiece is relatively small, causing the cross-section of the chip to vary as the tool advances in its path. The classical view of this chip formation mechanism considers the tooth path to be circular, and the thickness of the chip at the entrance and exit equal to zero, as it is given by Equation 2.1.

$$h(\phi) = f_z \cdot sin(\varphi) \tag{2.1}$$

Where h is the chip thickness, f_z [mm/tooth] is the feed per tooth, and φ [º] is the instantaneous immersion angle. However, based on the real trochoidal trajectory of the cutting edges, several

studies proposed a more realistic approach to the modelling of the uncut chip thickness; some considering the tooth runout and radial displacement, others based on the different tool orientations utilized in five-axis milling and others based on the different tool geometries, as in the case of ball end mills [41–47].

Depending on the required characteristics of the manufactured parts, the milling process can offer a large variety of solutions through the various types of advanced machines and tools available nowadays. Nevertheless, for the scope of this work, only slot milling will be further discussed.

The slot milling process is characterized by the combined action of an up milling stage and a down milling stage, as depicted in Figure 2.2.

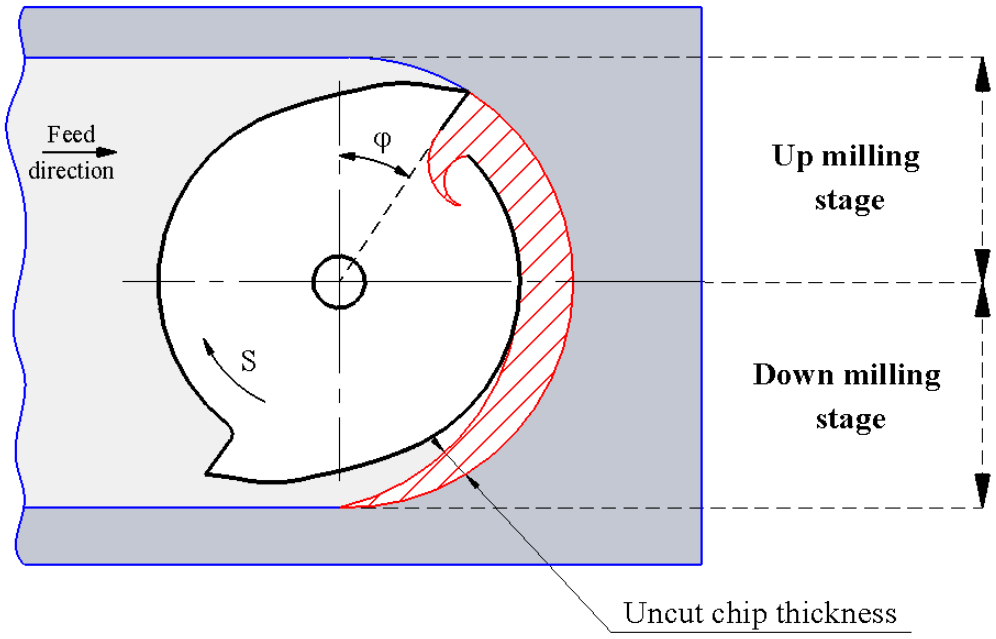

Figure 2.2 Slot milling

The first stage is marked by the increase in the thickness of the chips, resulting on the intensification of the cutting forces, until the instantaneous position angle reaches π/2 rad. Subsequently, when the position angle is between π/2 rad and π rad, the down milling stage occurs, being characterized by the reduction on the chip thickness and by the decrease of the forces required to remove material.

As it is known from the literature [48], the chip compression ratio, ζ, given by Equation (2.2), is a measure of the plastic deformation that occurs during the deformation of the chips that provides a correlation of the material properties with cutting performance resultant from machining.

$$\zeta = \frac{h_c}{h} \tag{2.2}$$

Where h_c [mm] corresponds to the thickness of the chip after the cut, and h [mm] is the uncut chip thickness.

This relation between the uncut chip thickness and the thickness of the chips after the cut, can also provide an insight on the cutting behaviour, through the shear angle, ϕ [º]. In fact, for the same amount of force, a higher shear angle implies that more material is being removed, resulting in more efficiency of the cutting process. According to the oblique cutting model, presented in Figure 2.3, this angle can be calculated through Equation (2.3).

$$tan\,(\phi) = \frac{\cos\,(\alpha_r)}{\zeta - \sin\alpha_r} \tag{2.3}$$

Where α_r [º] is the rake angle in the plane normal to the cutting edge, and its given by Equation (2.4).

$$tan(\alpha_r) = \; tan(\alpha) \cdot \cos(i) \tag{2.4}$$

In which, α [º] is the rake angle provided by the tool manufacturer, and i [º] the tool helix angle.

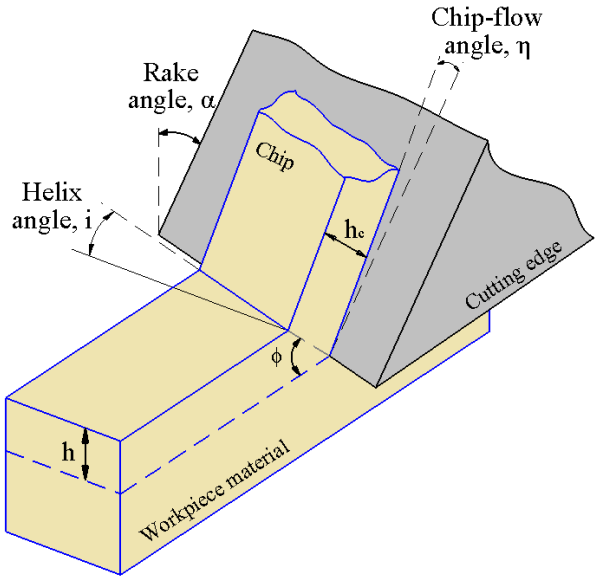

Figure 2.3 Oblique cutting model (Adapted from [49])

Another possible way to access to the shear angle is through the cutting forces. Considering the Merchant theory and assuming that the material is isotropic, Equation (2.5) provides the approximation of the shear angle for which the shear strain is at its maximum [48].

$$F_c = R \cdot sin(2\phi) \tag{2.5}$$

Where Fc [N] is the cutting force in orthogonal turning and R [N] is the resultant cutting force.

While turning an HSLA steel with uncoated carbide inserts, Sivaraman et al. [50] attributed the good machinability of the material to the microstructural constituents, composed mainly by bainite, martensite and polygonal ferrite, referring to the high strength of the material as factor that did not influence the cutting performance of the material, when compared with other grades of steels. A similar microstructure composed acicular ferrite, quasi-polygonal ferrite and bainite, of was also observed by Rodrigues et al. [10] on analogous WAAM thin-walled structures to those utilized in this study.

Concerning the properties that HSLA steels exhibit, namely, its good weldability and ductility, one of the major concerns during machining this type of steels is the development of a build-up edge (BUE). As explained by Ahmed et al. [51], the formation of BUE occurs when the compressive stresses, established between the tool-chip interface, cause the adhesion of highly strained material to the cutting edge.

In steady conditions, this adhered material may increase tool life, developing a build-up layer that protects the tool, and refine the quality of the surfaces by behaving as the cutting edge. Nevertheless, the resistance of BUE decreases with the increase of its size, causing it to break and to leave traces on the machined surfaces and chips. This mechanism occurs uncontrolled and cyclically, meaning that there is a continuous formation and removal of BUE on the tools, which has a significant effect on its integrity and wear state. Furthermore, as reported in the literature the formation and morphology of BUE changes accordingly with: the tool type and coating [52]; lubrification technique [53]; and cutting parameters, being often associated to low cutting speeds [54].

After performing the milling operations, the resultant surface texture contains waviness, roughness, lay, which is the direction of the predominant surface pattern determined by the production process, and other unexpected superficial defects [55]. From the literature [18,20,22,24–27,56], it was possible to verify that the most common parameter is the arithmetical mean deviation of the accessed profile, R_a, that can be calculated through Equation 2.11.

$$R_a = \frac{1}{lr}\int_0^{lr} |Z(x)|\, dx \tag{2.11}$$

Where $Z(x)$ is the height of the profile and l_r [mm] is the sampling length.

However, this parameter only quantifies the mean absolute magnitude of the peaks and valleys of the profile, not being sensitive to specific variations in height. Therefore, for the further characterization of the surface texture, other parameters can be utilized, such as the maximum height of the profile, R_z,

that quantifies the maximum distance between the highest peak and the lowest valley within a sampling length [57].

2.1 Chapter resume

From the literature review, it is possible to conclude that WAAM has great potential for enhancing the industrial world with a more efficient way to manufacture large metallic components. Despite some limitations are associated with this additive manufacturing technology, its combination with known subtractive techniques may provide the means to rapidly overcome such concerns.

For the development of the experimental work and posterior analysis of the results, some considerations must be taken into account. The anisotropic distribution of the mechanical properties of the WAAM parts and the residual stresses inherent to the WAAM process are important factors that may cause problems during milling. Also, it is important to notice that the properties of the workpiece material may also affect the cutting process.

In light of this issue, the influence of the physical processes behind milling on WAAM components is a subject that requires research, since it is known that different input parameters result in different mechanical characteristics on the manufactured parts. Thus, the importance of studying the interaction between WAAM and the milling process.

3

Experimental procedure

As discussed in the previous chapter, WAAM components exhibit poor surface quality and dimensional accuracy. In this study, the milling process is employed to overcome these defects.

Nevertheless, there are two concerns that may affect the removal of material. The first is related to the gradient of the mechanical properties inherent to the WAAM thin-walled parts and the second is due to the typical waviness developed during layer deposition.

For this reason, the removal of the outer layer, where the waviness represents a geometrical problem, is essential to exclude any concerns about the vibrations and instability on the tool caused by this characteristic of the thin-walled structure. Additionally, a milling strategy that isolates regions with similar mechanical behaviour is required.

In this chapter, the procedure and the characterization techniques employed for the manufacturing of the samples and the milling experiments are described.

3.1 Material specifications and samples manufacturing

Two different types of thin-walled structures were manufactured using the custom-built WAAM-GMAW equipment on the industrial technology laboratories of FCT-UNL, one corresponding to a high heat input and the other to a low heat input.

The deposition parameters employed for manufacture the samples are presented in Table 3.1 and were identical to those utilized in [10].

However, differing from the strategy selected to deposit the thin-walled structures, in this study a zig-zag approach was taken. With this approach the direction of the deposition was inverted at the end of every layer, promoting the development of a more levelled structure in terms of height [7].

In order to produce samples as identical as possible and to avoid distortions and geometric deviations, the thin-walled structures were deposited on mild steel substrates with 190×100×10 mm, which were cleaned prior to the depositions. The length of the walls was set to 150 mm and the height to 75 mm. These dimensions were specified in favour of the required number of tests and considering the fixture and the tool diameter.

Additionally, a distance of 7 mm between the torch and the substrate/previously deposited layer, an interlayer time of one minute and a shielding gas flow rate of 8 l/min, were kept constant in all depositions. The shielding gas composition is presented in Table 3.2.

Table 3.1 Process parameters utilized during the manufacturing of the samples (Adapted from [10])

Sample type	Current [A]	Voltage [V]	Travel speed [mm/s]	Wire feed speed [m/min]	Heat Input [J/mm]
High heat input	95	21	3.9	3	511
Low heat input	95	21	9	3	221

Table 3.2 Shielding gas composition

Shielding gas	Ar	H_2O	O_2	C_nH_m
Alphagaz 1	≥ 99.999%	≤ 3 ppm	≤ 2 ppm	≤ 0.5 ppm

The feedstock material in use was an EN ISO 16834-A G 69 4 M21 Mn3Ni1CrMo wire electrode from DRATEC, correspondent to a HSLA steel. Its chemical composition is presented in Table 3.3 and the mechanical properties are detailed in Table 3.4.

Table 3.3 Chemical composition of the feedstock material [wt%] [58]

C	Mn	Si	Ni	Cr	Mo	Fe
0.10	1.70	0.70	2.00	0.30	0.50	Balance

Table 3.4 Mechanical properties of the feedstock material [58]

Yield Strength [MPa]	Tensile Strength [MPa]	Elongation [%]	Impact energy [J]
880 – 920	940 - 940	20 - 16	95 - 65

3.1.1 Characterization of the additive manufactured parts

The characterization techniques of the thin-walled structures were made in order to guarantee that the different strategy employed during the deposition did not influence the microhardness and the mechanical behaviour of the material. For this reason, a section of the additive manufactured structures was cold mounted and etched with Nital (3% solution).
On the regions where the milling operations would be performed:

- The microhardness was accessed on a section of the thin-walled structures with a Mitutoyo HM-112 Micro-Vickers Hardness Testing Machine, a load of 0.5 kg was applied during 10 s;
- The microstructure was observed with an Olympus CX40RF200 optical Microscope.

Furthermore, the surface waviness was determined by acquiring the profile of the sections of the thin-walled structures with a scanner and analysing it with Adobe Photoshop CC 2018. The method employed for the waviness measurement was the same as in [59], where it is given by half of the difference between the maximum wall width and the effective wall width, as depicted in Figure 3.1.

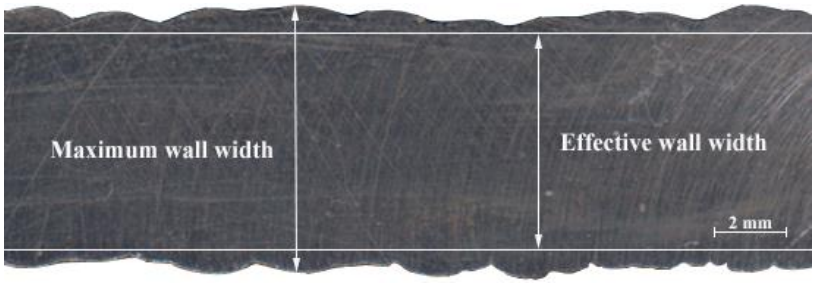

Figure 3.1 Method employed for waviness measurement

3.2 Milling operations

To prepare the samples for the milling operations, from each deposited structure two parts were removed with a mechanical hack saw. Later, the holes required for the fixture were made with a drilling machine and the resultant samples were ground until the complete removal of the surface waviness, as demonstrated in Figure 3.2.

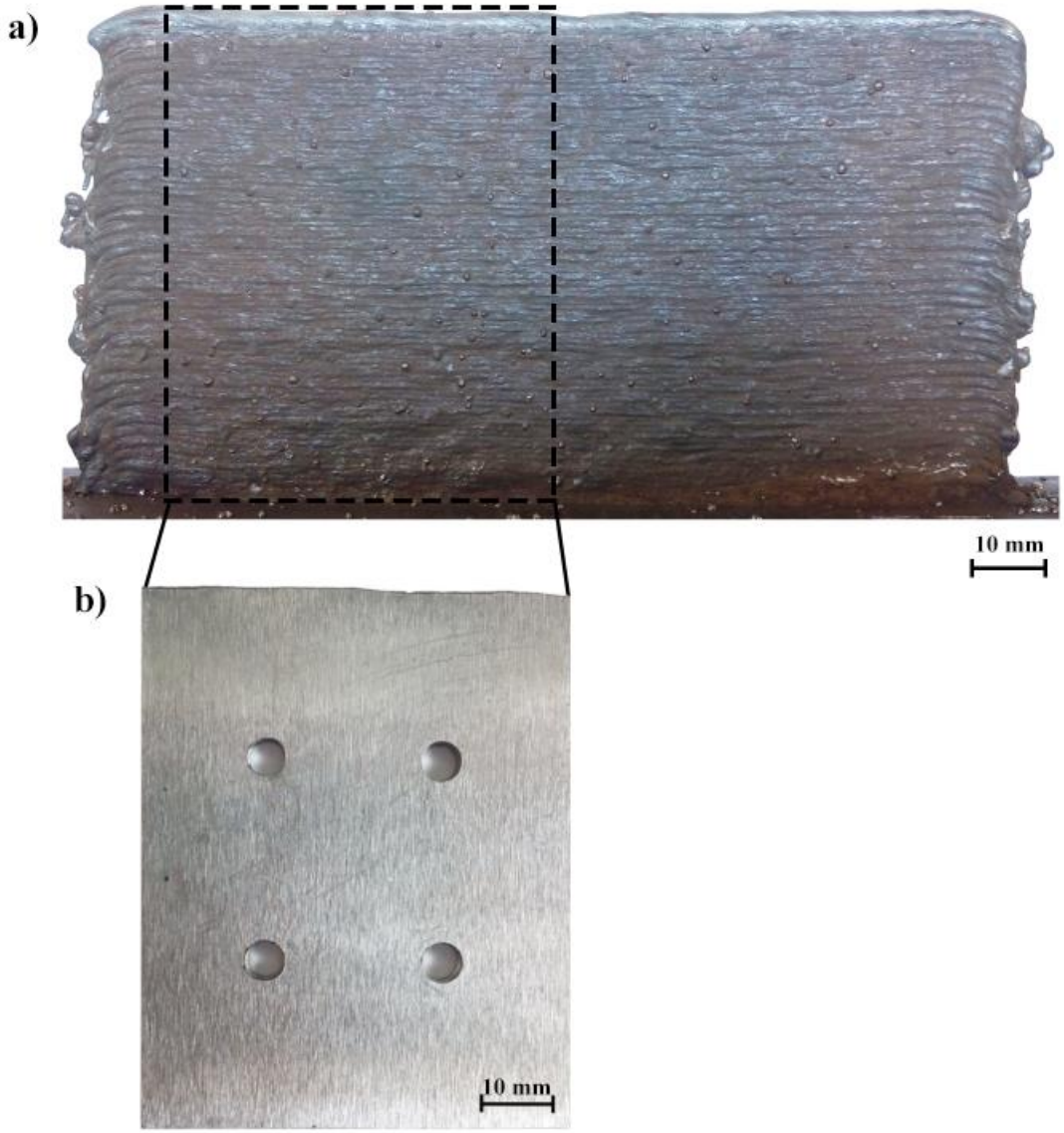

Figure 3.2 Sample preparation: a) Thin walled structure; b) Grinded sample

According to the measured and expected microhardness, the samples were divided into three regions: base, centre and top. With this in consideration, the influence of the cutting parameters was investigated with the milling of two slots per region, each with one passage of the tool, as presented in Figure 3.2.

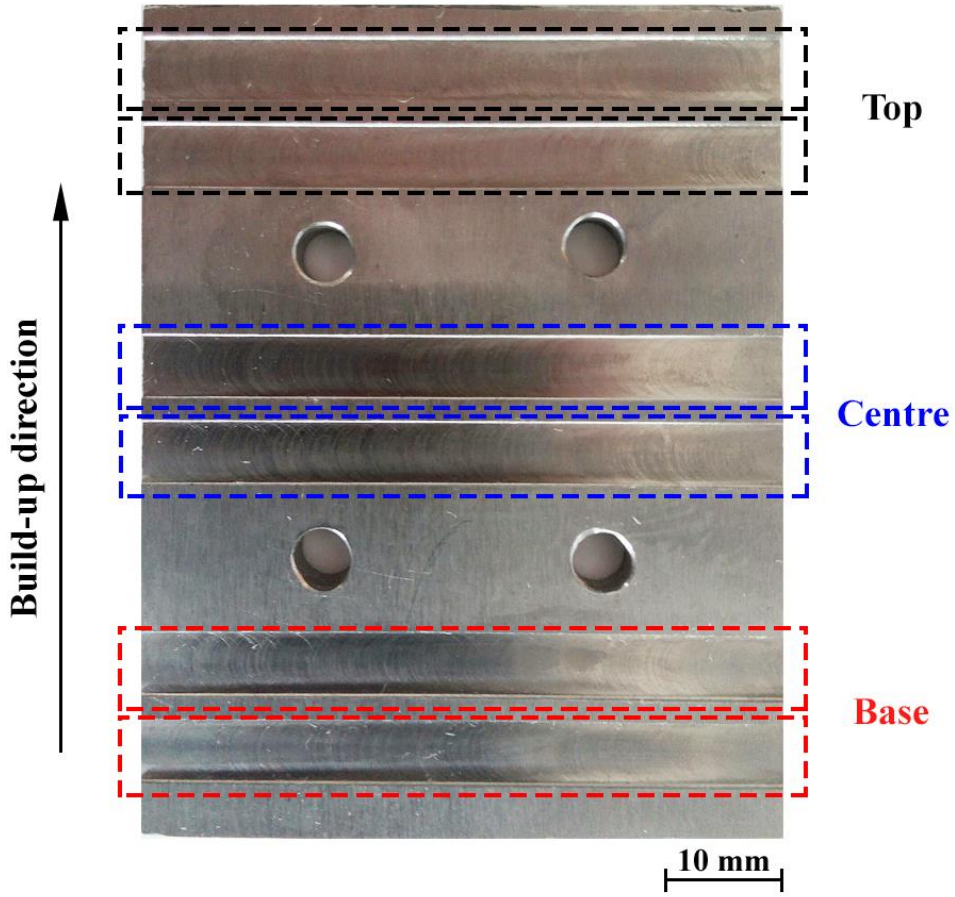

Figure 3.3 Milling strategy

In Table 3.5, the three levels of the feed per tooth and the cutting speed utilized in the experiments. These were selected based on the tool catalogue provided by the manufacturer, for different classes of steels. The axial depth of cut, however, was set constant to one-tenth of the tool diameter, 0.6 mm, and the established radial depth of cut was the same as the tool diameter, 6 mm.

Table 3.5 Levels of the cutting speed and feed per tooth

Parameters	**Levels**		
	Low	**Middle**	**High**
Cutting speed [m/min]	30	47.5	65
Feed per tooth [mm/z]	0.0115	0.023	0.0345

The several combinations of cutting parameters utilized during the experiments are summarized in Table 3.6. The order of the experiments was generated to minimize the setup time and at the end of one face, the samples were rotated, resulting in a total of six experiments per face. For every different sample, a new tool was inserted on the machining centre.

Table 3.6 Milling experiments

Experiment	v_c [m/min]	f_z [mm/tooth]	a_p [mm]	a_e [mm]	S [rpm]	F [mm/min]	t_m [s]	Region
# 1	30	0.0115	0.6	6	1592	36.61	98	Base
# 2	47.5	0.0115	0.6	6	2520	57.96	62	Base
# 3	30	0.0115	0.6	6	1592	36.61	98	Centre
# 4	47.5	0.0115	0.6	6	2520	57.96	62	Centre
# 5	30	0.0115	0.6	6	1592	36.61	98	Top
# 6	47.5	0.0115	0.6	6	2520	57.96	62	Top
# 7	65	0.0115	0.6	6	3448	79.31	45	Base
# 8	30	0.023	0.6	6	1592	73.21	49	Base
# 9	65	0.0115	0.6	6	3448	79.31	45	Centre
# 10	30	0.023	0.6	6	1592	73.21	49	Centre
# 11	65	0.0115	0.6	6	3448	79.31	45	Top
# 12	30	0.023	0.6	6	1592	73.21	49	Top
# 13	47.5	0.023	0.6	6	2520	115.92	31	Base
# 14	65	0.023	0.6	6	3448	158.62	23	Base
# 15	47.5	0.023	0.6	6	2520	115.92	31	Centre
# 16	65	0.023	0.6	6	3448	158.62	23	Centre
# 17	47.5	0.023	0.6	6	2520	115.92	31	Top
# 18	65	0.023	0.6	6	3448	158.62	23	Top
# 19	30	0.0345	0.6	6	1592	109.82	33	Base
# 20	47.5	0.0345	0.6	6	2520	173.88	21	Base
# 21	30	0.0345	0.6	6	1592	109.82	33	Centre
# 22	47.5	0.0345	0.6	6	2520	173.88	21	Centre
# 23	30	0.0345	0.6	6	1592	109.82	33	Top
# 24	47.5	0.0345	0.6	6	2520	173.88	21	Top
# 25	65	0.0345	0.6	6	3448	237.94	15	Base
# 26	65	0.0345	0.6	6	3448	237.94	15	Centre
# 27	65	0.0345	0.6	6	3448	237.94	15	Top

The selected tool for the tests was an uncoated carbide end mill S902 from DORMER, presented in Figure 3.3. Its specifications are presented in Table 3.7. This choice was based in order to fulfil the milling tests requirements and in order to have only one tooth in contact with the workpiece at a time. Additionally, an uncoated carbide tool is the most economical selection from a tool cost perspective for the machining of steels, hence it was chosen prior to coated or ceramic tools.

Figure 3.4 Tool dimensions [60]

Table 3.7 Endmill S902 specifications [60]

Material	Diameter	No. of teeth	Helix angle	Rake angle	Nose radius
Uncoated Carbide	6 mm	2	30 º	12 º	0.13 mm

To avoid any complications caused by instability of the cutting system, a fixture was developed to hold the samples in the correct position. It consists of a mild steel block with the dimensions presented in Appendix A. The samples were then clamped to it with four class 8.8 M4 screws and washers, with a torque of 1 Nm to achieve a good mechanical coupling.

3.3 Cutting forces acquisition

The milling experiments were performed in A.J. Maltez – Sociedade Metalúrgica, Lda., using an ecoMill 70 machining centre from DMG MORI.

During the milling tests, the cutting forces were measured utilizing an acquisition pathway composed of a multicomponent dynamometer Kistler 9257B, a Kistler 5070 multichannel charge amplifier, a DAQ system and a computer with LabVIEW software. A schematic representation of the experimental setup utilized during the cutting forces measurement is shown in Figure 3.4. The coolant utilized during the experiments was compressed air.

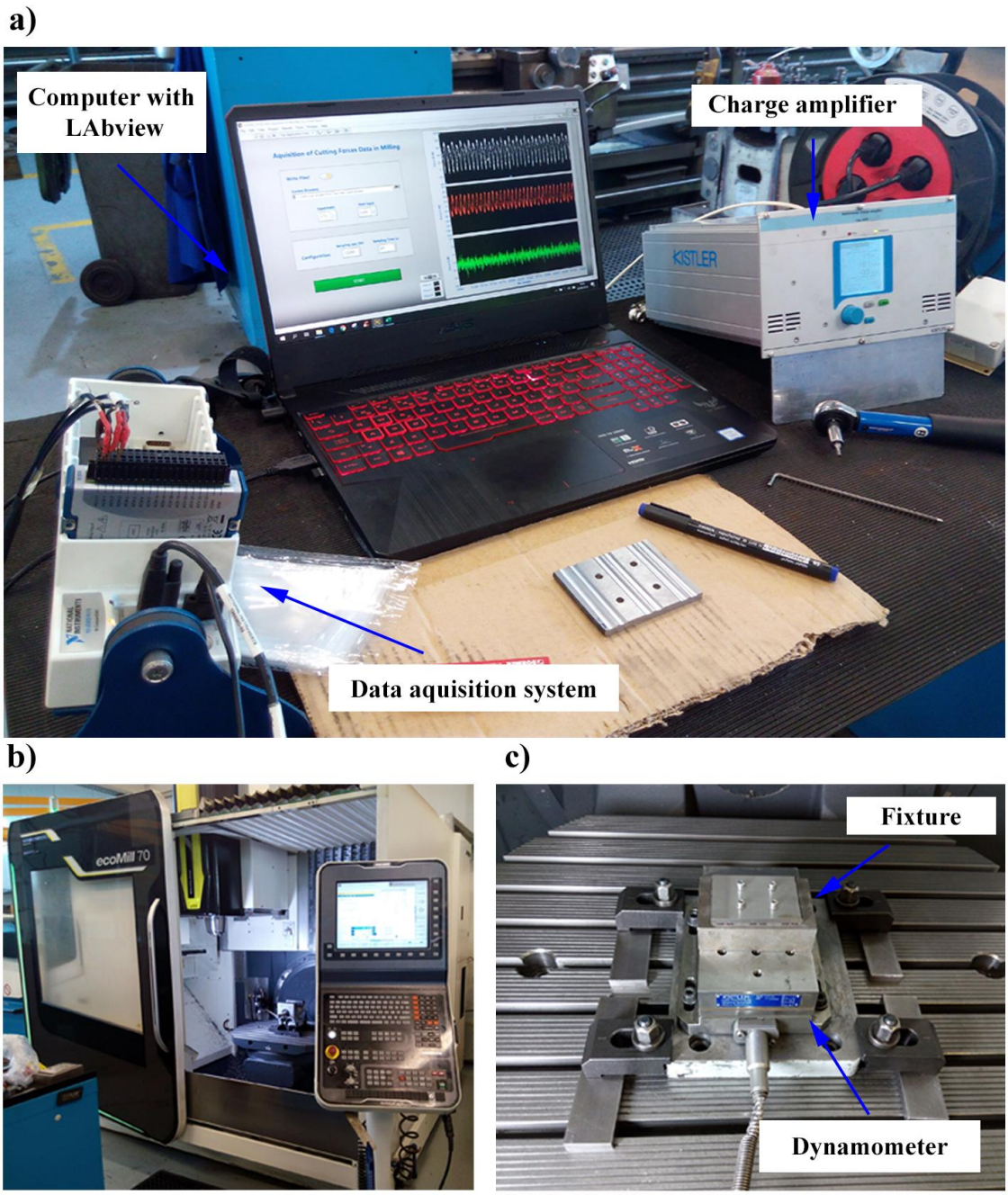

Figure 3.5 Experimental setup: a) Signal acquisition pathway; b) ecoMill70 Machining centre; c) Fixture and dynamometer

The multicomponent dynamometer Kistler 9257B consists of four piezoelectric sensors, each comprising three pairs of quartz plates, one responsive to pressure in the z-direction and the other two sensitive to shear in the x and y directions. There are fourteen M8×1.25 threaded holes to which the fixture is fastened.

The Kistler 5070 multichannel charge amplifier converts the force measurement electric signal into a proportional voltage that is conditioned in the DAQ system, composed of a NI 9205 module and a NI cDAQ-9178 chassis. The data is then acquired through LabVIEW software, that converts the

input voltage into a measurement of force, newton, N, and later processed via MATLAB R2019a software

In this LabVIEW program, the sampling rate and sampling time are defined in order to specify the number of samples required to record all the cutting data. It also provides the means to organize the information thought the selection of the name, according to the cutting parameters and location of the output .txt files; the correspondent block diagram is presented in Appendix B.

3.4 Characterization techniques

Surface quality analysis

The surface roughness parameters R_a and R_z were measured in the direction normal to the feed with a stylus-based profilometer MarSurf PS 10 from Mahr, in accordance with ISO 4288 standard [61].

Five measurements with an evaluation length of 0.25 mm were performed in three regions of the machined surfaces, at the middle and near the tool entrance and exit. Additionally, the ratio between R_z and R_a was calculated.

Additionally, the machined grooves were observed closely at the Olympus CX40RF200 optical microscope in order to examine the resultant quality of the surfaces.

Tool integrity analysis

To evaluate the wear mechanisms on the tools utilized during the milling experiments, these were observed with a Leica DMI5000 M optical microscope. The characterization of the tool wear was made in accordance with 8688-2 standard [62].

Chip analysis

The chips from each machined slot were gathered when the tool was, approximately, on half of its pathway. The chip morphology was observed at the Leica DMI5000 M optical microscope.

The thickness of the chips was measured, and the chip compression ratio was calculated with Equation 2.2.

Milling performance analysis

The shear angle was computed based on the chip measurements using Equation 2.3 and based on the cutting forces, using Equation 2.5.

4

Results and Discussion

In this chapter, the results obtained during the experiments are presented and discussed.

In a first instance, the results of the characterization of the AM parts are examined in order to assess and verify the inherent characteristics and properties of the thin-walled structures produced with WAAM.

Secondly, the roughness tests outcomes and an analysis of the surface quality are presented.

The performance of the milling tests is evaluated through the cutting forces and resultant tool integrity.

The results from the chips analysis are then presented, followed by the results from the computation of the shear angle.

4.1 Characterization of the WAAM structures

The low heat input structures required an average of 72 layers to reach the 75 mm of height and presented a surface waviness of 687 ± 156 µm. Additionally, to manufacture the high heat input structures, only an average of 63 layers of material was needed, which exhibited a lower surface waviness of 551 ± 104 µm. Furthermore, the deposition strategy applied during the manufacturing process proved to be suitable in accomplishing a structure that is capable of achieving the geometrical requirements for the samples.

The resultant thin-walled structures from the WAAM process are presented in Figure 4.1. Here, the difference in width between the two types of thin-walled structures is noticeable, which is attributed to the distinct values of travel speed utilized during the manufacturing process, that resulted in a different amount of material being deposited in each layer [10].

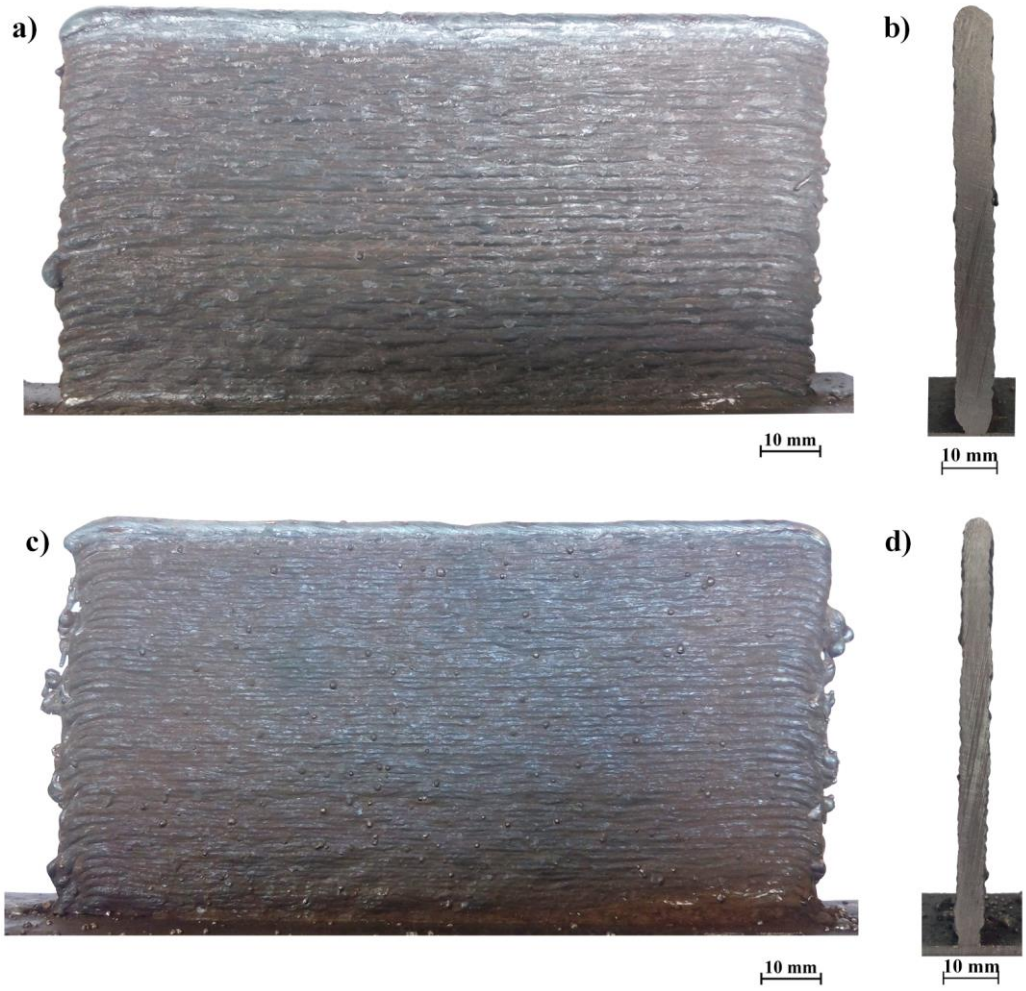

Figure 4.1 Thin-walled structures manufactured with WAAM: High heat input: a) Front view; b) transverse section; Low heat input: a) Front view; b) Transverse section

After removing the superficial waviness through grinding, the ready to machine samples acquired a final thickness of 2.8 mm for the low heat input specimens and 5.5 mm for the high heat input type. The resultant samples can be observed in Figure 4.2.

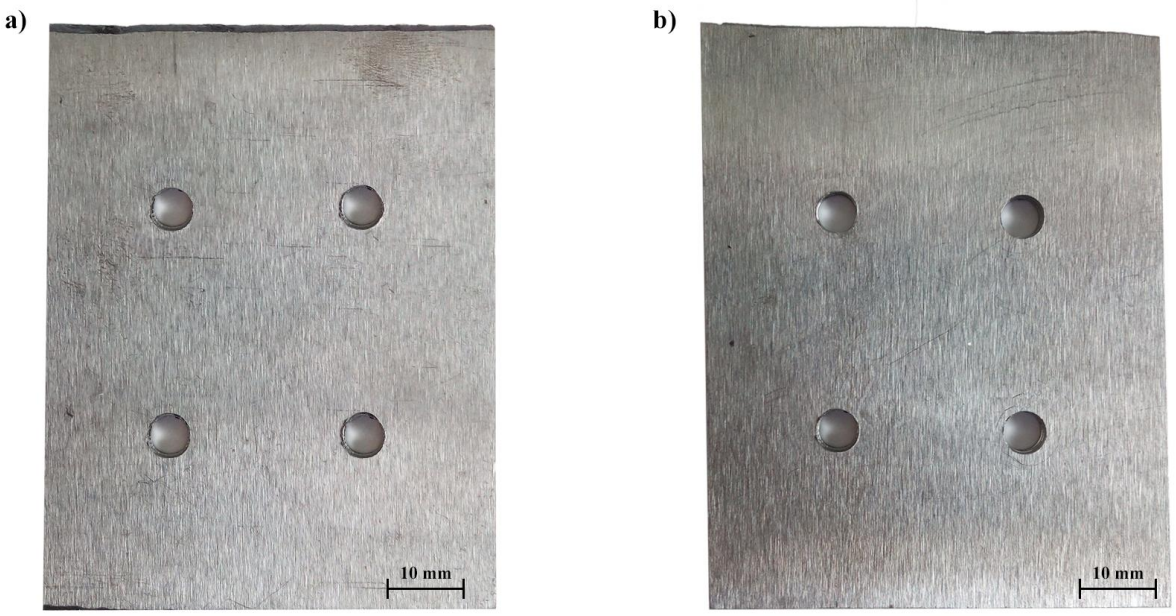

Figure 4.2 Prepared samples fos the milling operations: a) High heat input; b) Low heat input

In Figure 4.3 are presented the hardness measurements in the regions to be machined.

Both types of structures exhibited a gradient on the hardness profile that decreased along the height of the walls. As explained in chapter 2, this hardness gradient is due to the cooling rate and solidification process that, in turn, provide the conditions for the development of a gradient on the mechanical properties of the produced walls. As a result of a lower heat input utilized for manufacturing, the low heat input specimens exhibited a more uniform distribution of hardness than the high heat input structures.

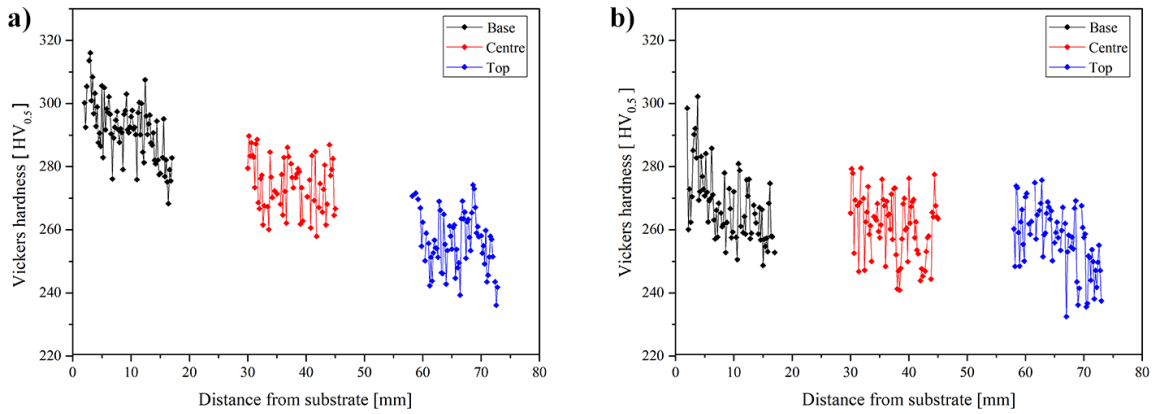

Figure 4.3 Hardness variation on the WAAM structures: a) High heat input; b) Low heat input

The microstructure of both thin-walled structures is presented in Figure 4.4. Here it can be observed that the grain size increases with the increase of height. This is highly noticeable for the high heat input case. In the low heat input structures, however, only a slight increase in the grain size can be observed, explaining the different hardness measurements between the samples. All these results are in good agreement with those expected from the literature [10]. Hence, no further investigation was made towards the characterization of the thin-walled structures.

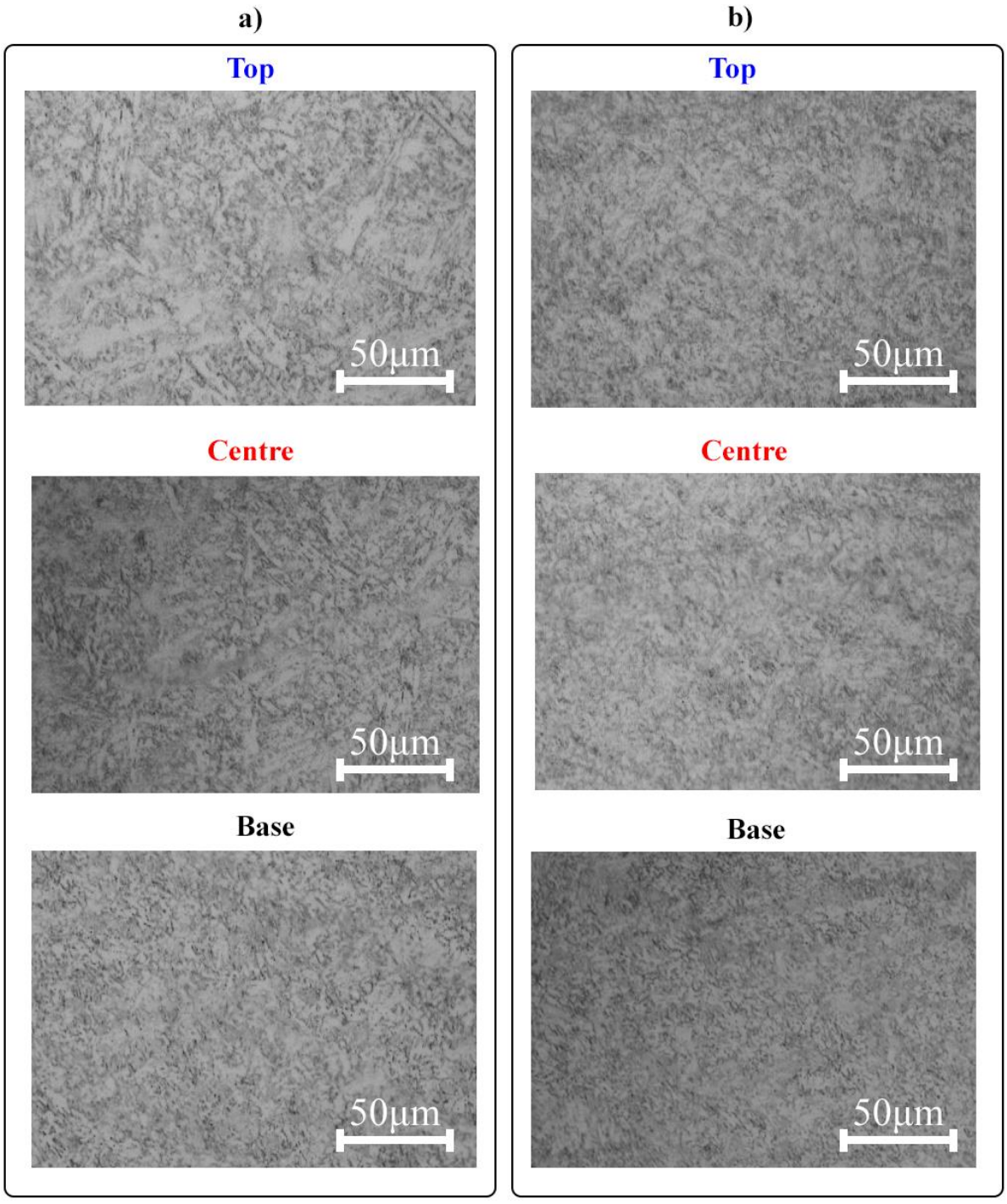

Figure 4.4 Microstructure: a) Low heat input samples; b) High heat input samples

4.2 Results from the surface integrity analysis

4.2.1 Surface defects on the machined grooves

A close look on the machined grooves revealed several defects on the surface topography. Both the low heat input and high heat input samples showed similarities on the types of defects that were found on the surfaces.

At a macroscopic level, it was observed the occurrence of sideward burrs at the periphery of the grooves and exit burrs at the end of the machined grooves, as depicted in Figure 4.5. Burrs can be classified based on their mechanism of formation and are a major concern on the machined parts quality, presenting several concerns on industrial safety and component assembly.

The top milling burrs are resultant from the plastic flow of the material when compressed and are related to high ductility of the workpiece material that grants it the ability to sustain severe plastic deformation without fracturing. At the same time, exit burs are generated when the workpiece material is pressed and deformed, instead of sheared at the exit of the tool [63,64]. These burrs, however, can be removed with a subsequent deburring operation.

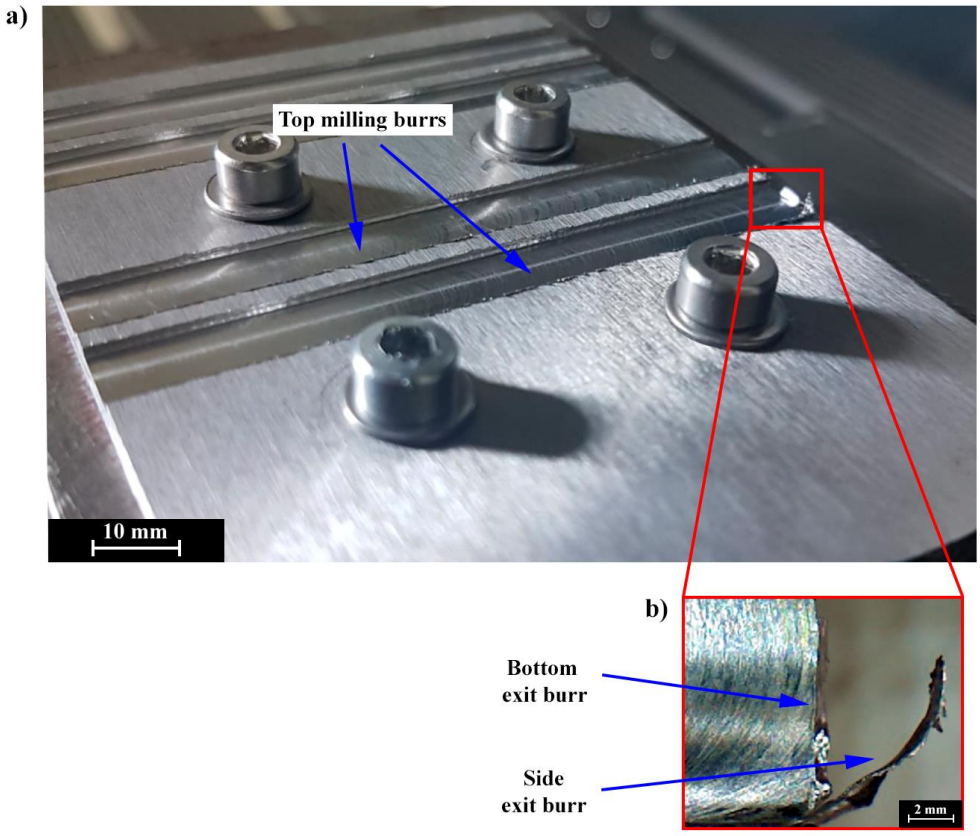

Figure 4.5 Occurrence of burrs on the machine grooves: a) Top milling burrs; b) Exit burrs

Microscopically, the presence of adhered material on the machined surfaces was also noticeable. This is due to the formation of a build-up edge (BUE) at the tool/chip interface, that at certain levels of strain becomes unstable resulting on the adhesion of small fragments of material on the surfaces [51]. Additionally, the presence of an up-milling stage during slot milling, which causes the carrying and re-cutting of chips, aggravates the BUE formation mechanism. The presence of this adhered material on the surfaces was also reported by Sivaraman et al. [50] while turning a HSLA steel.

The density of this build-up edge residue on the surfaces differed according with the process parameters in use, provided that the stability and geometry of the build-up edge varies accordingly with various factors, as established in Chapter 2. In Figure 4.6 is represented the magnitude of this defect resultant from experiment 8 of the high heat input samples.

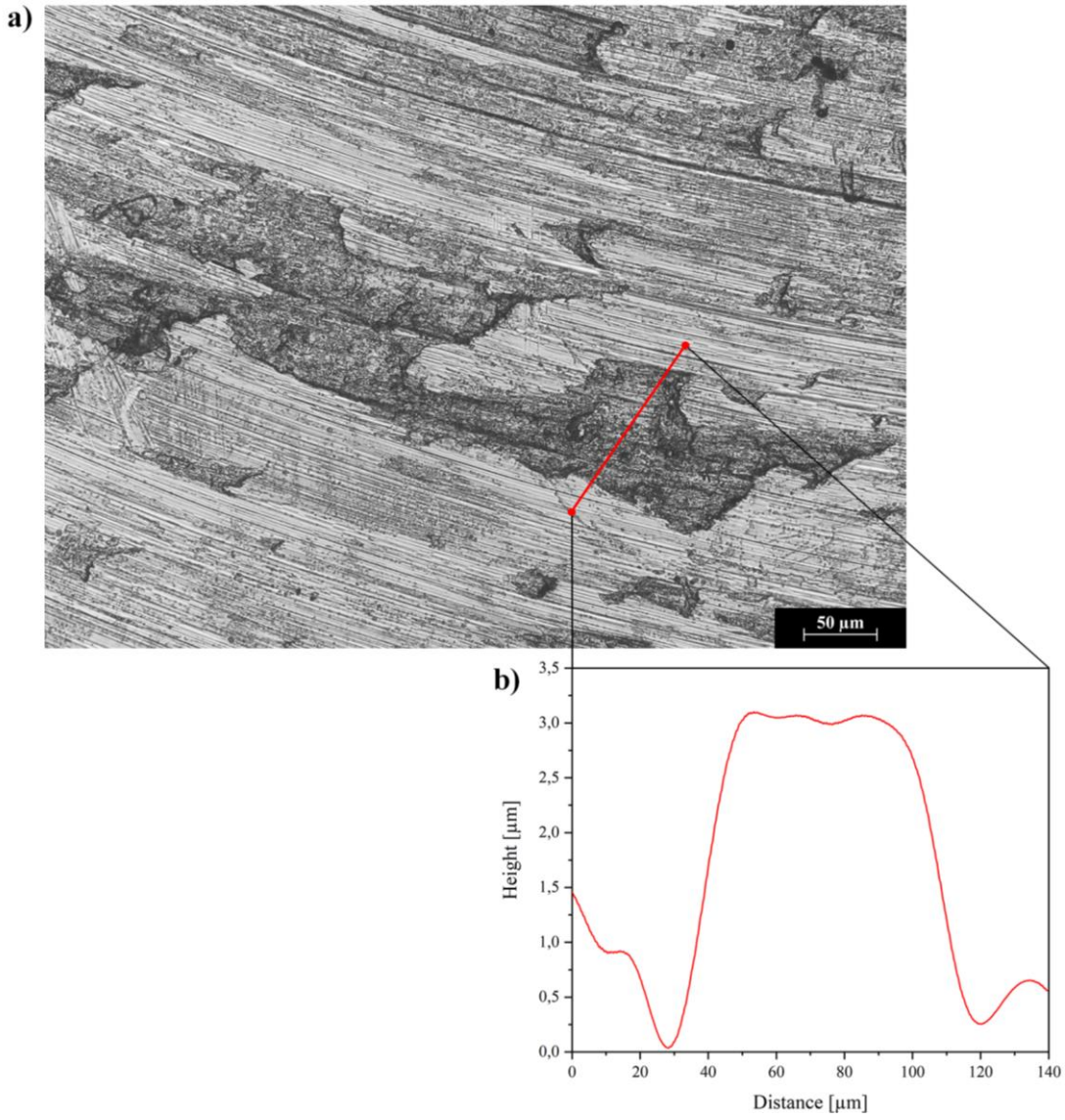

Figure 4.6 Adhered material on the machined surfaces: a) Machined surface with v_c = 30 m/min; f_z = 0.023 mm/tooth; base region; high heat input samples; b) Profilometric analysis to determine the height of the adhered material

Other superficial defects can also be observed, as detailed in Figures 4.7 and 4.8. The feed marks, which are characteristic from the milling process, are resultant from the advance of the tool, indicating the direction of lay. Differences on this type of defects were noticeable when altering the cutting parameters. Nevertheless, the surfaces that exhibited feed marks without substantial density of other defects were found when using a high cutting speed and a low feed per tooth values. Additionally, differences were also found when varying the machined region (base, centre or top). This can be due to the wear state of the tool, which can be resultant from the applied milling strategy or be an evidence that the characteristics of the WAAM parts affect the cutting process.

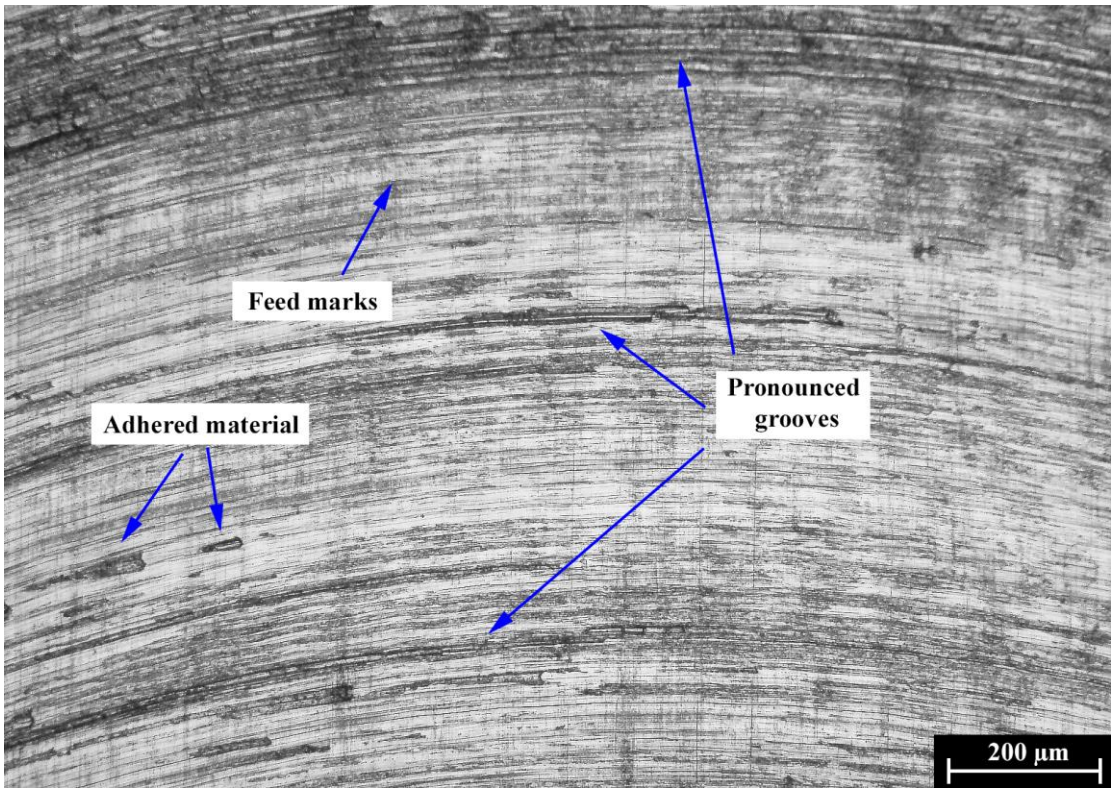

Figure 4.7 Defects on the surface topography: experiment 6 on the low heat input samples

Pronounced grooves were also observed. These are caused by the increased friction between the tool and the workpiece material, that in turn is influenced by factors such as the tool integrity and BUE formation and stability.

The side flow of material was also visible. This phenomenon is characterized by the plastic deformation that occurs during the compression of the tool against the workpiece, that causes the material to flow to the sides instead of being removed. It was observed that the increase in feed caused this type of defect to be more noticeable. From another perspective, it can also be influenced by the tool wear state, since a more deteriorated tool increases the contact area between the tool and

the workpiece, resulting on more friction being developed and thus more temperature is generated, increasing the ductility of the material [65].

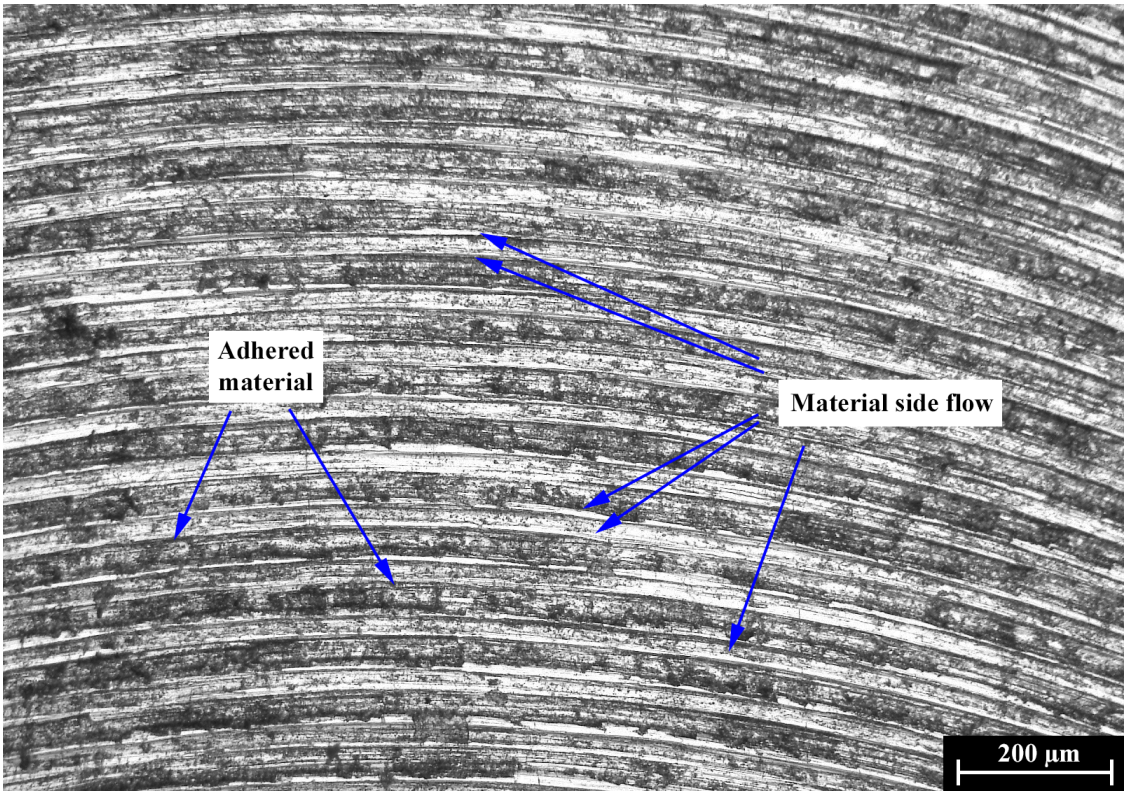

Figure 4.8 Defects on the surface topography: experiment 23 on the high heat input samples

As depicted in Figure 4.9, the main differences on the surface integrity of the two heat input samples occurred at experiment 12, evidencing different wear conditions on the tools, that will be discussed later in this document. The presence of a groove on the opposite direction of the lay means that one tooth is more deteriorated than the other, causing differences in height between the teeth.

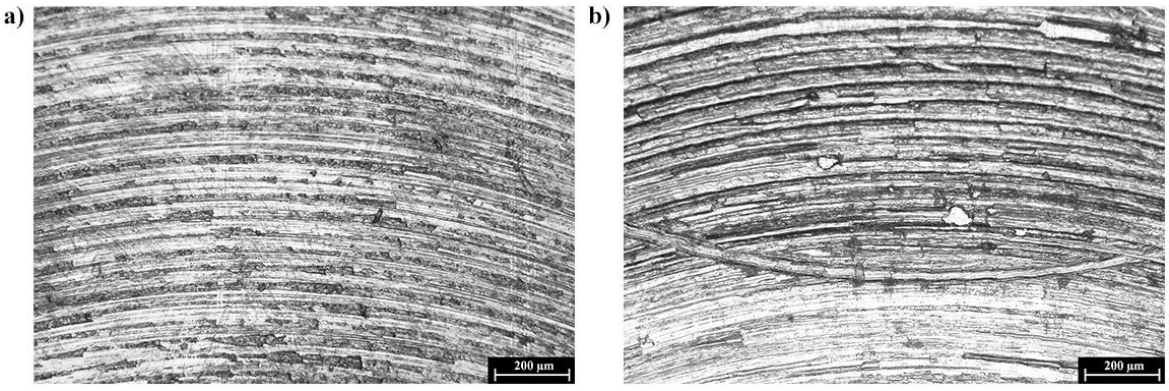

Figure 4.9 Surface integrity after experiment 12: a) Low heat input samples; b) High heat input samples

4.2.2 Results from Ra parameter measurements

In Figure 4.10 the variation on the Ra parameter is presented for the three machined regions. All the roughness measurements on both types of samples are presented in Appendix D.

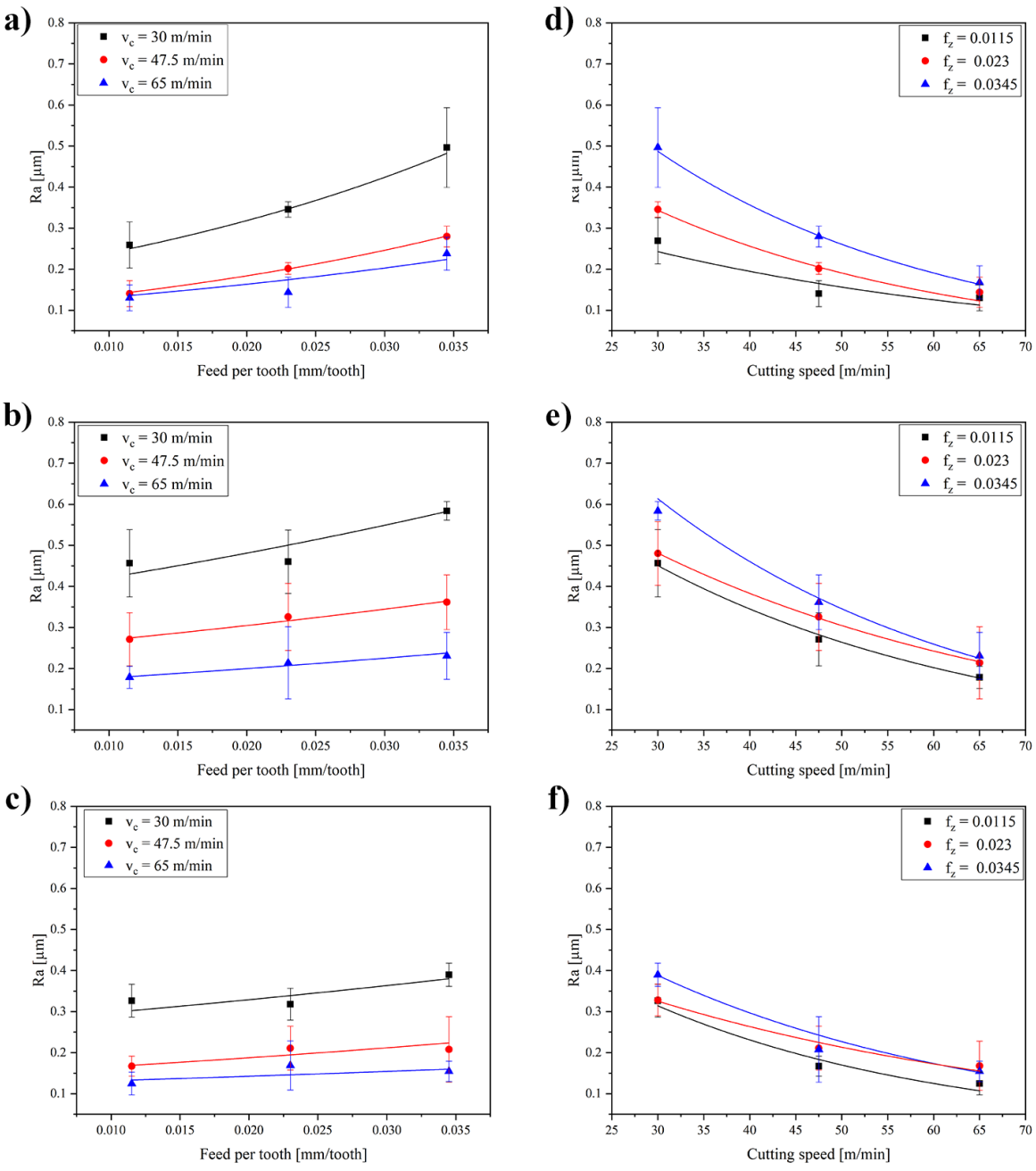

Figure 4.10 Trend behaviour of the surface roughness on the low heat input samples: a) Influence of the feed per tooth on the top; b) Influence of the feed per tooth on the centre; c) Influence of the feed per tooth on the base; d) Influence of the cutting speed on the top; e) Influence of the cutting speed on the centre; Influence of the cutting speed on the base

From Figure 4.10 a), b) and c), it is possible to observe that the surface roughness increases with the increase of the feed per tooth.

Additionally, when machining with higher cutting speeds the effect of the feed per tooth is practically unnoticeable. The opposite occurs when machining at low cutting speed, where the surface roughness is more scattered. This can be attributed to the friction developed between the tool and the workpiece. At low cutting speeds, less friction occurs and thus the temperature developed during the cut is lower, meaning that more force required for the removal of material and the probability for BUE to occur increases.

Analysing Figure 4.10 d), e) and f), a decrease on the values of the Ra parameter can be observed when increasing the cutting speed.

Overall, on low heat input samples, the influence of the cutting speed is the parameter that yielded a more noticeable effect on the Ra measurements.

4.2.3 Results from Ra parameter measurements of the high heat input samples

On the high heat input samples, similar trends to those observed on the low heat input samples were observed, although the roughness values are more dispersed. The higher values for the surface roughness were achieved at the top region. This difference can be attributed to the wear condition of the tool, as a result from the applied milling strategy, the residual stress state on the WAAM parts, or the higher gradient of hardness. Additionally, the increase of grain size towards the top influences the ductility of the material, that in turn affects the formation mechanisms of BUE.

The high dispersion of values does not allow for the accurate analysis of the cutting mechanism on the high heat input samples. For instance, in Figure 4.12 a), when machining with a cutting speed of 47.5 mm/min, the correspondent experiments are experiment 6, experiment 17 and experiment 24. Such experiments were performed after milling other regions with different sets of process parameters. Experiment 6 occurred after machining at low cutting speeds, where the formation of BUE was expected. Experiment 17 corresponded to a different tool which was subjected to higher cutting speeds, and thus the adhesion of material would not present such a detrimental effect on the tool. In the case of experiment 24, however, the higher surface roughness could be attributed to the increased state of wear, being the last experiment where the same tool was utilized.

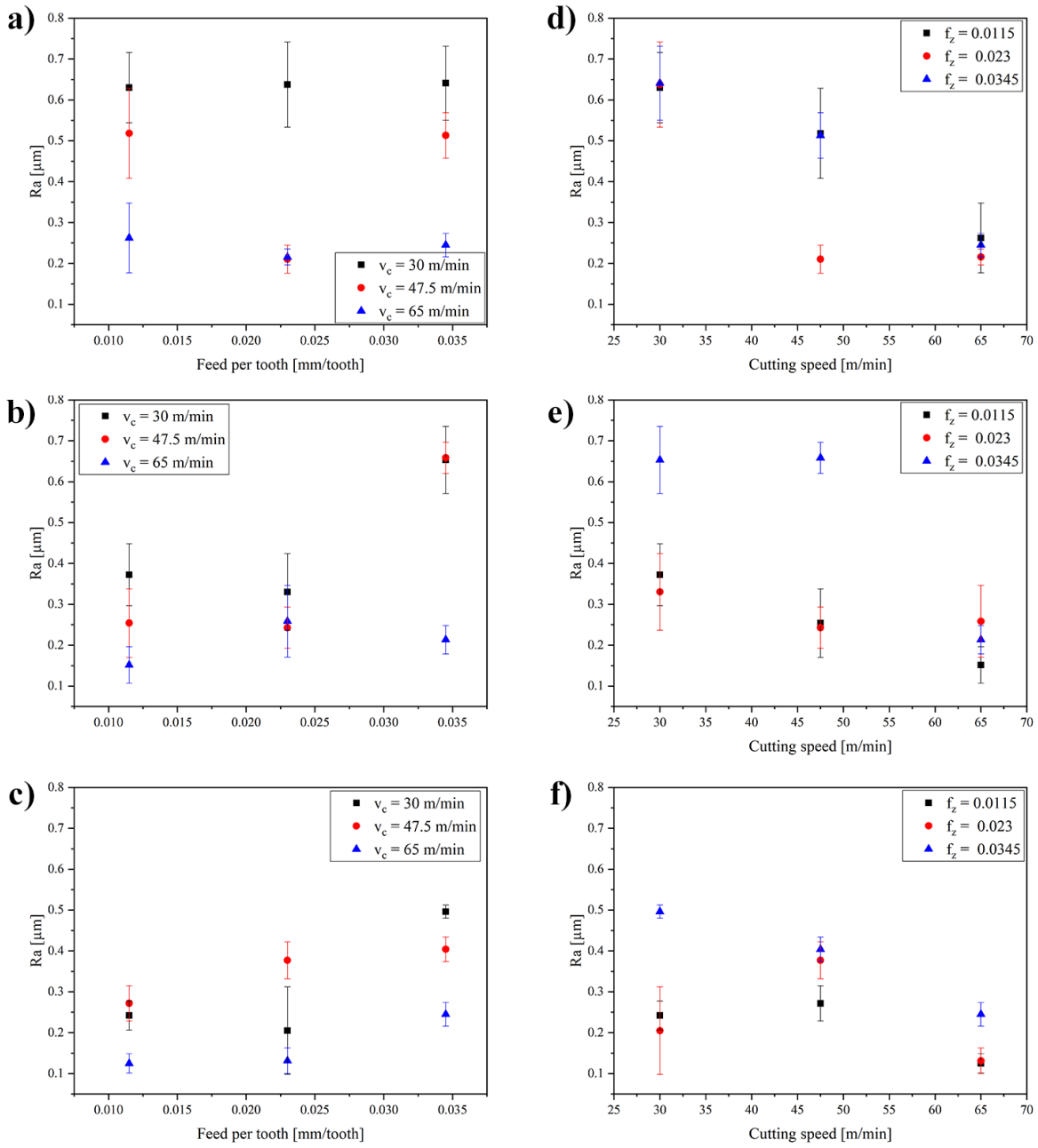

Figure 4.11 Trend behaviour of the surface roughness on the high heat input samples: a) Influence of the feed per tooth on the top; b) Influence of the feed per tooth on the centre; c) Influence of the feed per tooth on the base; d) Influence of the cutting speed on the top; e) Influence of the cutting speed on the centre; Influence of the cutting speed on the base

4.2.4 Results from Rz parameter measurements

In Figure 4.12 are exhibited the fluctuations of the Rz parameter in the three regions for both types of samples. Being highly sensible to variations in height or in depth, this parameter can provide an insight on the regions that were more influenced by the different cutting parameters. The experiments specifications are available in Table 3.6.

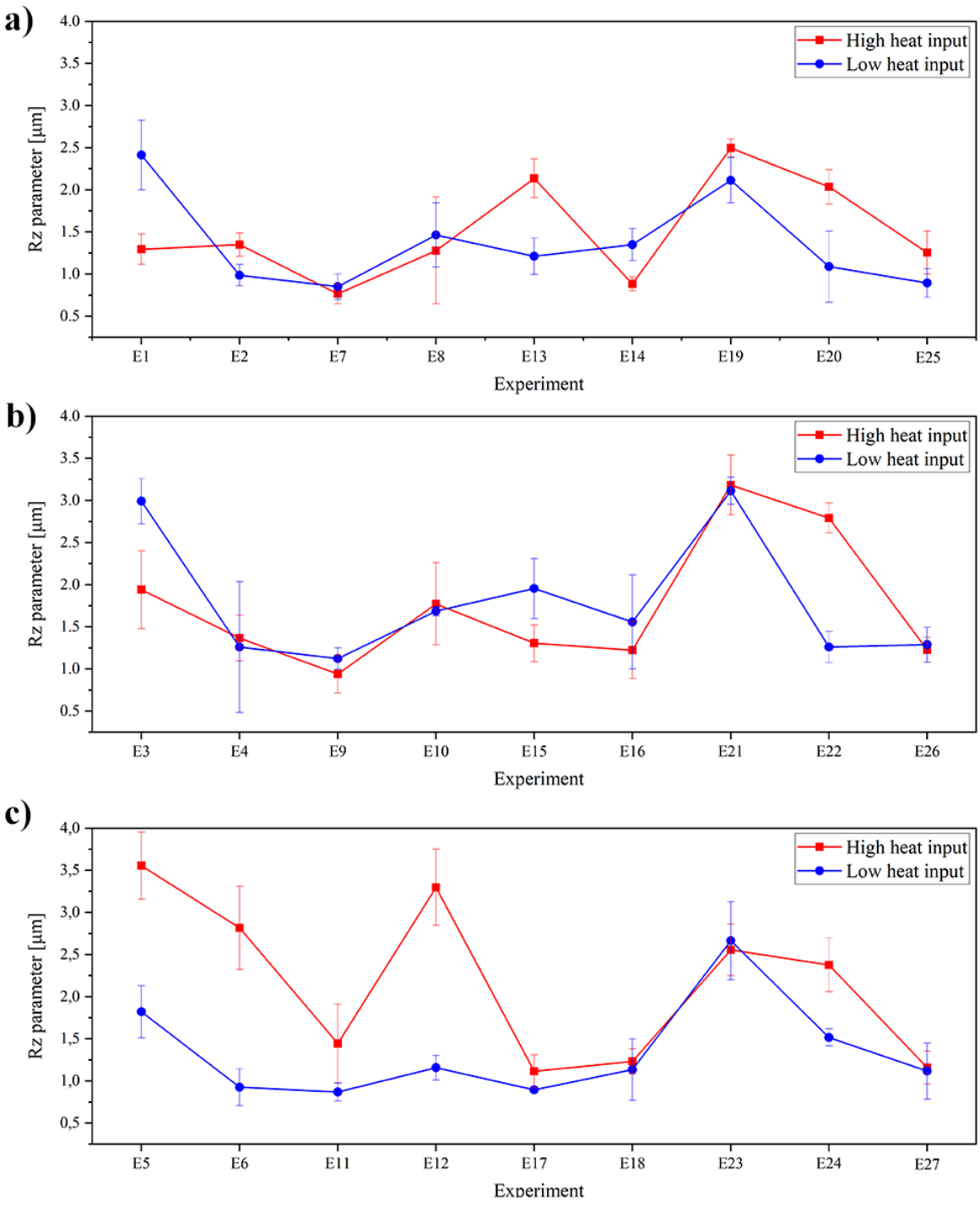

Figure 4.12 Rz parameter measurements: a) Base region; c) Centre region; c) Top region

In the base and centre regions, the maximum height of the Rz parameter profile is practically the same. However, comparing the high heat input and the low heat input samples, it can be observed that in the top region there is a higher discrepancy in the measured values. This may be indicative of the influence of the metallurgical characteristics inherent to the WAAM parts on the cutting process, as it is known from the literature that differences in grain size and in the mechanical properties result on the variation the cutting forces and differences on the tool integrity, which are important factors on the resultant roughness [66,67].

Nevertheless, with exception to experiment 12, where the tool wear condition had a significant effect on the surface, experiment 5 and 6, correspondent to lower values of cutting speed and feed per tooth, also exhibit a high value for this parameter, being followed by a decrease on the Rz value at experiment 7, while machining with the same tool. This phenomenon may evidence the influence of the characteristics of the WAAM parts on the milling process on the formation of BUE or in the wear state of the tool.

4.2.5 Analysis of the Rz/Ra ratio

The values of the ratio between Ra and Rz near the tool entrance, at the middle of the cut and at the exit of the tool, are presented in Table 4.1.

The ratio between Rz and Ra is practically constant in all the machined grooves. This evidences that the performance of the milling operations remains stable throughout the milling operations, at the regions where the roughness was measured in a groove, and that the applied fixture and the wear condition of the tool had similar behaviour throughout the experiments.

The values range from 4.13 to 7.55 for the low heat input samples and from 4.24 to 6.73 for the high heat input samples, for different experiments. The variation in these values evidence that the tool integrity, the cutting parameters and the overall cutting system resulted on different superficial characteristics that influence the roughness measurements, as observed previously.

Nevertheless, it is important to notice that this ratio does not provide any information on the roughness measurements of the samples, it only allows for the comparison of the cutting performance and stability in terms of the roughness profile, on the machined surfaces.

Table 4.1 Ratio between Rz and Ra parameters on different areas with identical cutting conditions

Experiment	Low heat input samples			High heat input samples		
	Near tool entrance	Middle	Near tool exit	Near tool entrance	Middle	Near tool exit
# 1	5.06	6.25	5.37	5.00	5.36	4.96
# 2	5.73	5.90	6.48	5.74	4.96	5.45
# 3	5.28	5.19	5.00	5.07	5.21	5.38
# 4	6.10	7.37	7.00	5.72	5.38	5.43
# 5	5.61	5.89	5.96	5.01	4.97	4.92
# 6	6.20	6.58	6.36	5.24	5.44	5.07
# 7	7.25	6.82	6.84	5.92	6.13	6.52
# 8	6.35	5.27	5.82	5.86	6.24	5.25
# 9	6.38	6.30	6.36	6.48	6.21	5.54
# 10	6.80	5.45	5.17	5.28	5.37	5.49
# 11	5.40	5.79	5.70	5.43	5.50	4.96
# 12	5.80	4.68	6.00	4.92	5.18	5.44
# 13	5.26	5.74	6.20	5.80	5.67	5.39
# 14	5.72	5.10	4.53	6.19	6.73	6.34
# 15	4.20	4.20	4.13	5.53	5.38	5.04
# 16	4.90	6.40	6.61	4.56	4.73	4.79
# 17	6.12	5.91	6.23	5.19	5.30	5.63
# 18	5.37	6.93	5.75	4.78	5.71	5.81
# 19	5.46	5.42	4.93	5.05	5.03	4.94
# 20	4.59	5.24	5.16	4.87	5.04	5.07
# 21	5.24	5.08	5.08	4.38	4.87	4.65
# 22	5.67	4.83	5.18	4.31	4.24	4.28
# 23	5.30	4.70	5.10	5.22	4.64	4.89
# 24	5.00	5.42	5.04	4.93	4.63	4.64
# 25	5.76	5.79	5.84	6.06	5.13	5.28
# 26	6.15	5.58	5.91	5.66	5.74	5.48
# 27	7.55	6.65	7.38	6.08	6.15	6.03

4.3 Results from the cutting forces acquisition

The resultant cutting force developed on a tooth during face milling can be divided in three components. In the active cutting plane, the projection of this force on the feed direction is the feed force, perpendicular to this direction is the feed normal force. On the direction normal to active cutting plane, is the axial component, the passive force.

Figure 4.13 depicts the three components of the cutting force before and after filtering with a Butterworth low pass filter. This way a clear measurement of the cutting forces can be achieved, by removing the high frequencies associated with the machine-tool, dynamometer and electric signal.

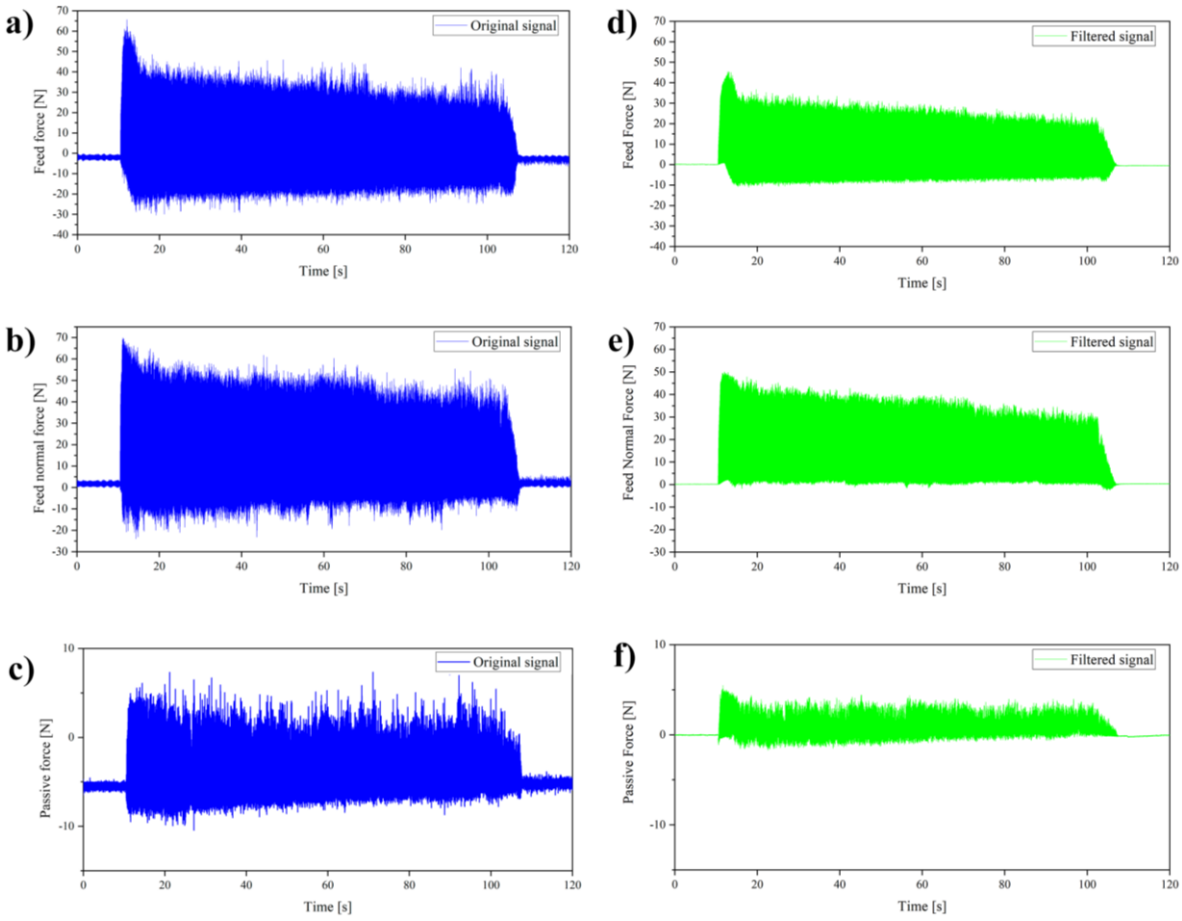

Figure 4.13 Cutting forces measurement signals from the experiment 5 on the high heat input samples: a) Original feed force signal; b) Original feed normal force signal; c) Original passive force; Corresponding filtered signals d), e) and f)

After computing the three components into the resultant cutting force, the final signal is presented in Figure 4.14 a). Here it is possible to observe that the behaviour of the cutting forces is composed of three stages. Firstly, when the tool is entering in the workpiece material, characterized by the increase

of the cutting forces. Secondly, a stable stage, where the cutting force is practically constant. Finally, when the tool is exiting the cut, a third stage, where a decrease on the cutting force can be observed.

At the stable stage, it can be observed the decrease on the magnitude of the resultant cutting force throughout the cut. This is due to the increase of the temperature, that resulted from plastic deformation that occurs during the chip removal before the fracture. Additionally, the vibrations caused by the formation of BUE and other factors can also be noticed, through the irregular peaks on the cutting force.

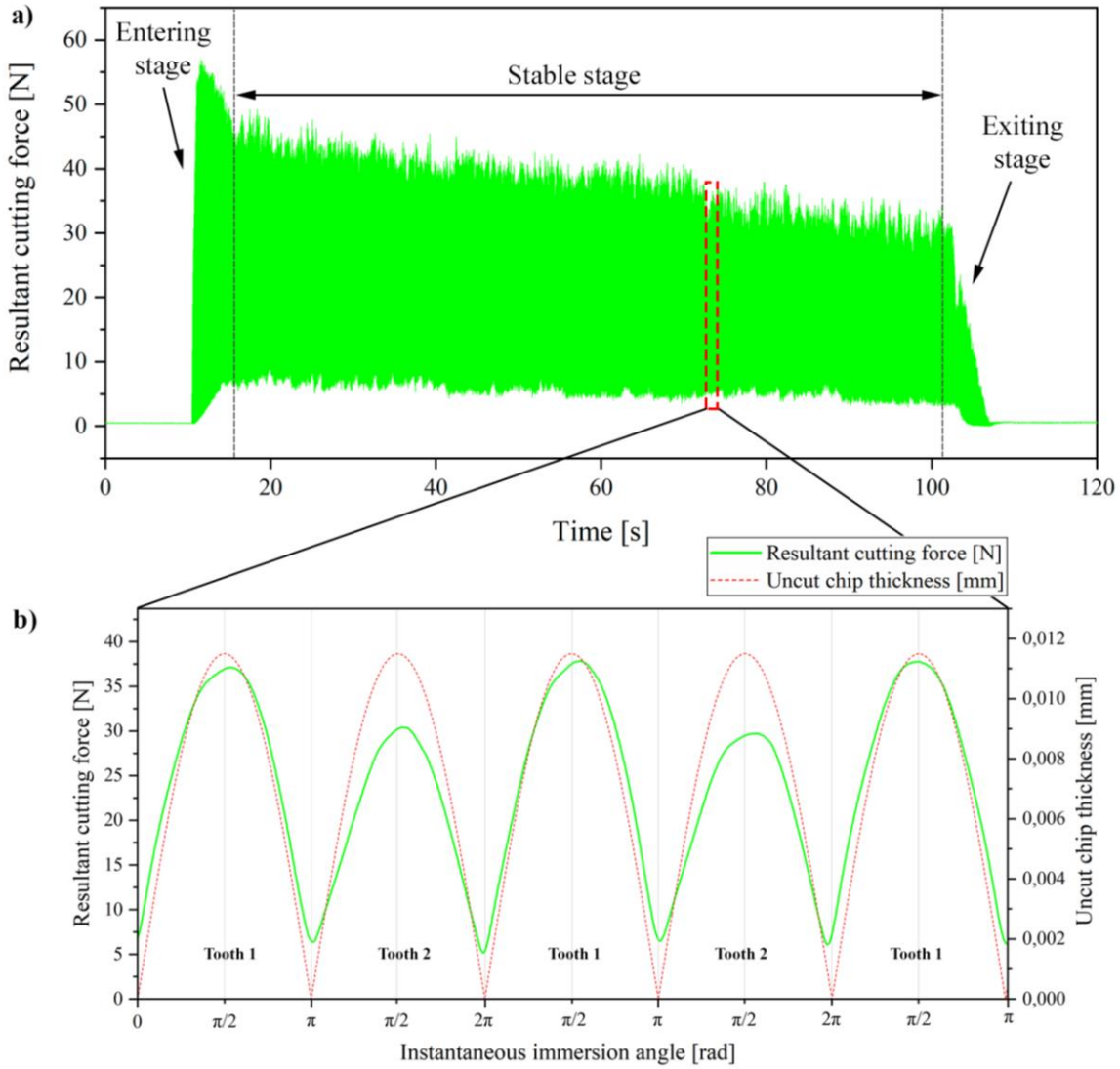

Figure 4.14 Resultant cutting force from experiment 5 on the high heat input samples: a) Computed signal; b) Intermittent cutting behaviour vs. uncut chip thickness

A closer look at the signal of the resultant cutting force (see Figure 4.14 b)) reveals the intermittent cutting action caused by the continuous variation of the uncut thickness of the chip during the slot milling operations in the workpiece, as explained in chapter 2. Here the behaviour of the cutting force

exerted by the tool, composed of two teeth, is compared with the classical view of the uncut chip thickness.

While varying with time, the instantaneous immersion angle dictates the relative position of the cutting edge during the removal of a chip, making it possible to separately observe the two cutting stages comprised in slot milling.

On a tooth, the first stage can be observed when the instantaneous immersion angle varies between 0 rad and $\pi/2$ rad, where an increase on the magnitude of the cutting force occurs until a maximum is reached. This is caused by the increase on the chip thickness as the tooth advances on its path. The second stage is characterized by the decrease on the resultant cutting force magnitude and uncut chip thickness until, the exit of the tooth, at π rad. At the same time, however, the second tooth enters in the workpiece having a similar behaviour to that of the first tooth.

Furthermore, it can be observed that the maximum cutting force achieved in each tooth differs. This feature occurs due to the runout caused by the tool fixture and other geometric deviations on the tools.

4.3.1 Maximum resultant cutting force performance

The maximum cutting force developed during milling was detached from the resultant cutting force graphics, on the stable stage of the cut. The results of these values are depicted in Figure 4.15 and are presented in Appendix E.

From Figure 4.15 a), b) and c) it can be observed that the increase of the cutting speed results on the reduction of the cutting forces, which can be explained by the increase of the friction at the tool/workpiece interface that results on the increase of temperature, that eases the material removal process.

Additionally, as depicted in Figure 4.15 d), e) and f) increasing the feed per tooth results on the increase of the cutting forces, which is due to the increased compression of the tool on the workpiece.

Overall, the three regions behaved in a similar manner, leading to similar conclusions reported by [50], that the high strength of the material, or in the presented case the gradient of hardness that influences the mechanical properties of the material, did not yield a significant effect on the cutting force performance.

When machining the high heat input samples, a similar performance to that of the low heat input samples was observed, however, the measurements do not provide accurate conclusions due to the uneven distribution of the measured values. This variation on the maximum cutting force measurements can be due to the combined effect of the tool wear condition, the BUE formation

mechanisms and to the milling strategy taken in this study. Additionally, the top is the region where the cutting force measurements presented more scatter, as in the roughness measurements case.

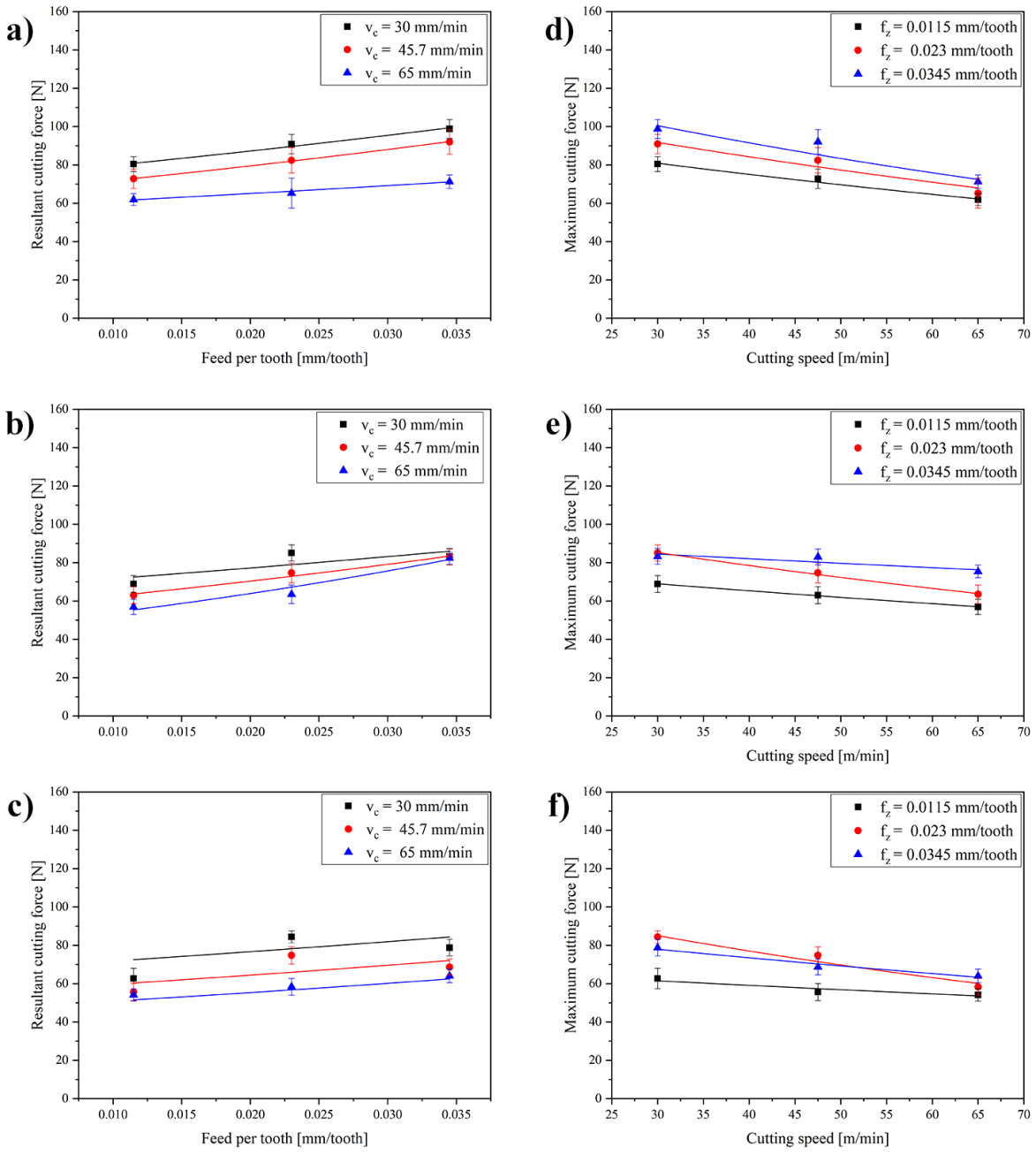

Figure 4.15 Tendencial behaviour of the maximum resultant cutting force on the low heat input samples: a) Influence of the feed per tooth on the top; b) Influence of the feed per tooth on the centre; c) Influence of the feed per tooth on the base; d) Influence of the cutting speed on the top; e) Influence of the cutting speed on the centre; Influence of the cutting speed on the base

4.3.2 Overall cutting force performance on the first set of experiments

Figure 4.16 depicts the different magnitudes that the cutting forces acquired throughout the experiments, where the roughness measurements presented more dissimilarities. The experiments are detailed in Table 3.1.

As presented in chapter 3, experiments 1, 2, 3, 4, 5, 6, 7, 9 and 11 correspond to the lower level of feed per tooth with different cutting speeds and in different regions, while experiments 8, 10 and 12 correspond to the medium level of feed per tooth.

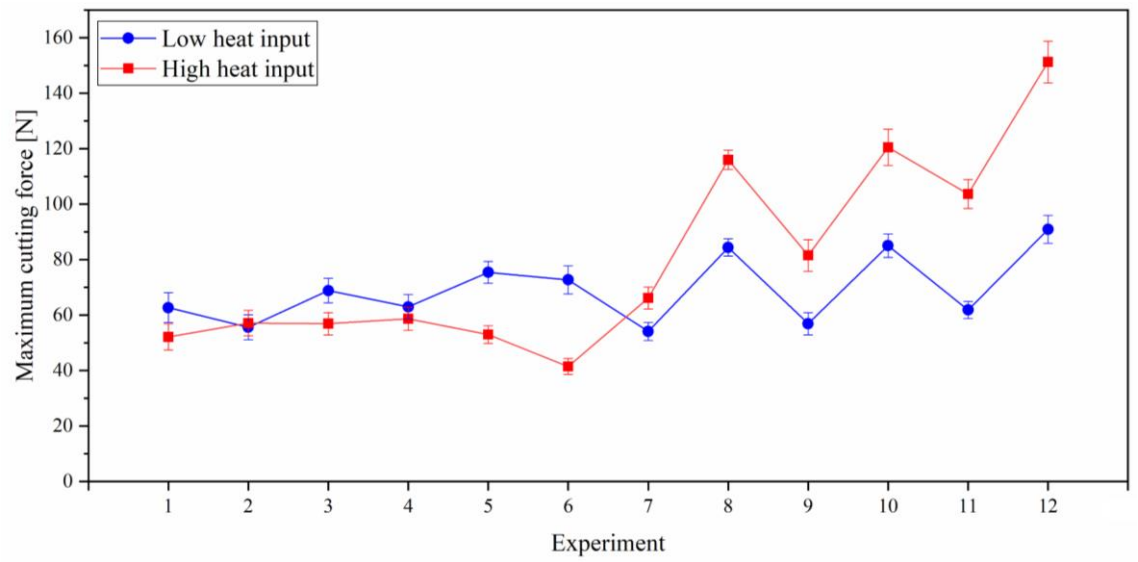

Figure 4.16 Overall cutting force performance on the first sample

Here it can be observed that, on the low heat input case, the cutting forces are constant depending on the cutting parameters in use. However, on the high heat input samples, the tool wear had a significant impact on the cutting forces.

The tools are characterized by having three stages of wear. The first stage correspondent to a rapid degradation of the cutting edge. Tthe second stage, where a steady-state of wear occurs. The third stage, however, is characterized by a severe and rapid degradation of the cutting edge. Although the tool wear is a phenomenon that cannot be avoided, it can be controlled through intensive research on the tool life.

On the first set of experiments, it is possible to observe that the major effect on the cutting forces of the high heat input case was due to the tool wear. Although it is not possible to specify accurately the corresponding experiments, from the presented information it is possible to observe that the third stage occurs somewhere after experiment 8.

Based on this information, another difference that can be observed between the two types of samples is in the magnitude of the maximum cutting forces correspondent to the experiments 5 and 6, which occurred at the top region, evidencing that the different characteristics of both samples have significance in the cutting process.

On the high heat input samples, a decrease on the maximum cutting force can be observed as a result of the decrease in hardness on the top layers.

On the low heat input case, however, the hardness does not exhibit such a significant variation, as a slight increase on the maximum cutting force can be observed, meaning that other factors have influence on the cutting process. Such can due to the increase in grain size, as Olovsjö and Nyborg [67], stated while machining nickel based alloys, where it was verified that the cutting forces increased with the increase in grain size. Another study presented by Olovsjö et al. [68] concluded, while studying the effect of the grain size and hardness on the tool wear condition, that the relation between the grain size and the uncut chip thickness affects the deformation of the chips and asserting that larger grains are associated with larger serrations on the chips.

However, the residual stresses state at the top region can also be the cause for this increase on the cutting forces, nevertheless, the residual stresses on WAAM parts are a subject that is still being subjected to intensive research.

4.4 Results from the tool observations

Although the experimental procedure is not applicable to the study of tool life, some conclusions can be drawn from the resultant integrity of the tools. In the present study, the major differences on the surface quality between the two types of samples occurred at low cutting speeds. A close inspection on the correspondent tools showed significant differences on the tool state of wear. With this in account, it is possible to perceive that the metallurgical aspects between the two types of samples exhibited a different behaviour on the tool wear mechanisms that occurred during machining.

Figure 4.17 and 4.18 depicts the wear condition of the flank faces of the tools utilized for machining the samples correspondent to the worst surface roughness.

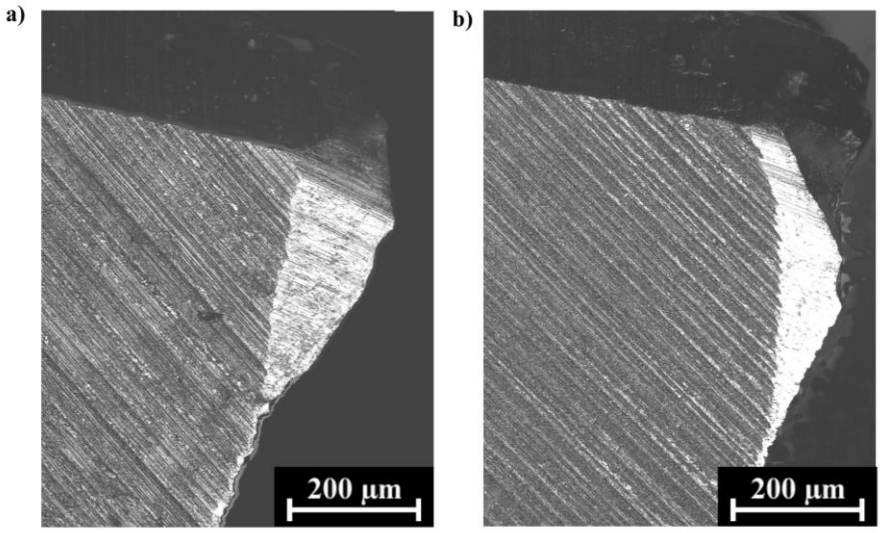

Figure 4.17 Minor flank face after experiment 12 : a) Low heat input; b) High heat input

On the low heat input samples, the maximum measured flank wear was 0.227 ± 0.029 mm. In this case, this value did not exceed the 0.3 mm maximum limit imposed by the ISO standard for tool life [62]. The flank face of the tool is practically intact, meaning that the tribological conditions resultant from the inherent characteristics of this type of samples, allows for good machinability on a tool wear perspective.

In the case of the high heat input samples the mechanisms that control the tool degradation, behaved in a different form. As it would be expected it can be observed a higher magnitude of wear on the flank. However, flank wear was not the tool life delimiter in this case. It can also be observed the fracture of small fragments of the tool, the degradation of the tool nose, and the adhesion of material. Nevertheless, the detrimental effects on the surfaces, caused by the facture of the tool nose, were only noticeable for the experiment 12 of the high heat input samples, which explains the correspondent high Rz value on Figure 4.12 c).

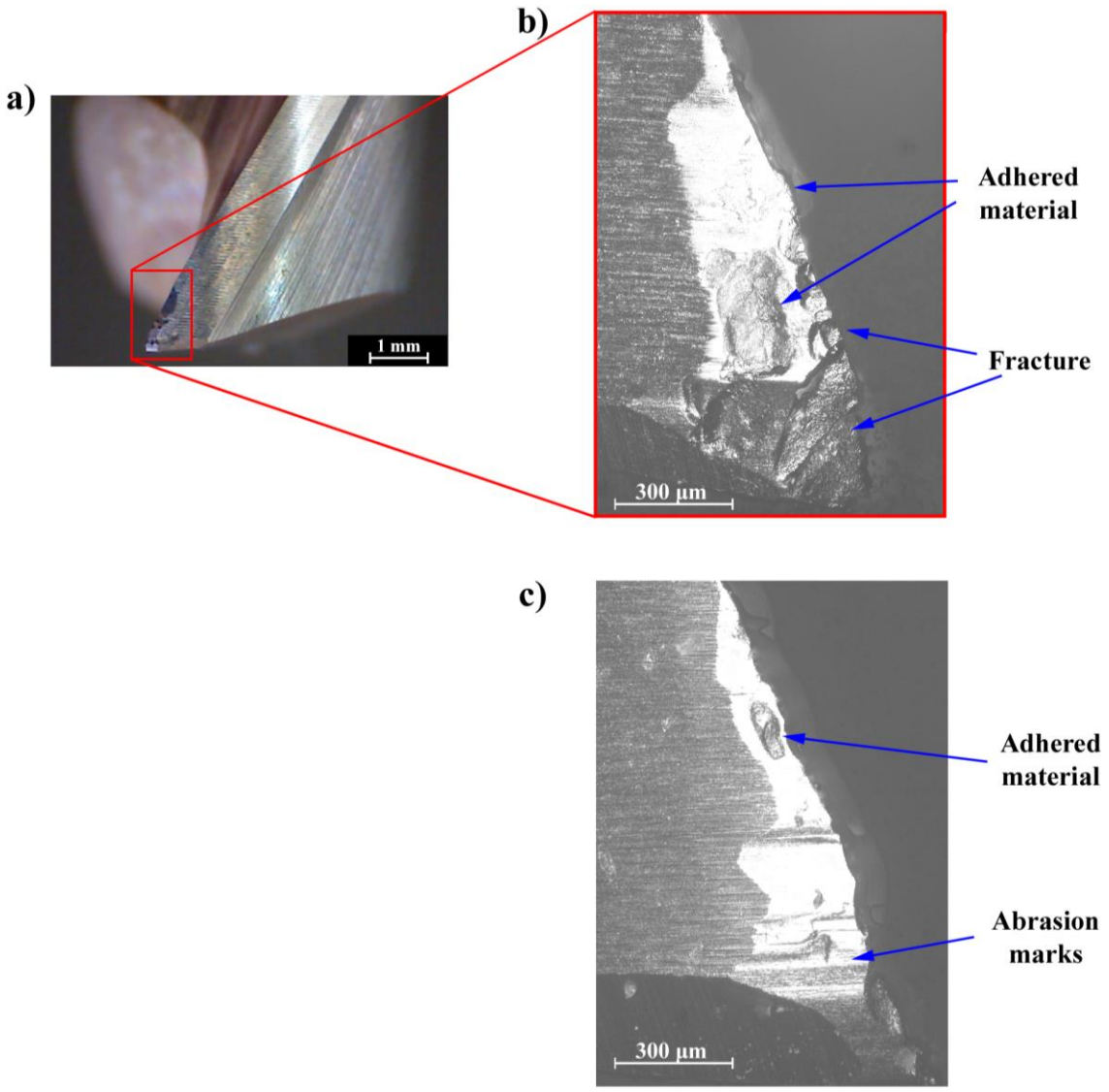

Figure 4.18 Major flank face after experiment 12: a) Tool wear resultant from machining the high heat input samples and b) detail of the corresponding view; c) Detailed view of the tool wear resultant from machining the low heat input samples

At low cutting speeds, the main wear mechanisms responsible for the degradation of the tools, are due to the combination of low temperatures with the high ductility and the good weldability of the workpiece material, that provides the conditions for the adhesion of material to the tool.

This results on the formation of BUE, that when stable can improve the quality of the surfaces, or in the development of a build-up layer, that protects the tool against the abrasion caused by the strain hardened chip fragments. Nevertheless, the instability of this adhered material on the tool/workpiece interface causes the friction between the surfaces to increase, intensifying the abrasion on the surfaces of the tool.

At higher cutting speeds, the increase in temperature reduces the formation of BUE, when at least the temperature of recrystallization is reached [48]. Nevertheless, with the rise of temperature, the diffusion of chemical compounds between the tool and the workpiece may also have a significant influence the tool wear rate. This, in turn, is an influential factor on the development of a crater at the rake face of the tool, which until a certain depth can be beneficial to the surface integrity, by sharpening the cutting edge.

The increase of temperatures, however, is not particular to high cutting speeds, being influenced also by the friction conditions imposed by the characteristics of the workpiece material. This is a possible explanation for the loss of the tools cutting edge during the milling operations on the high heat input samples, since that it is an influential factor on the development of crater wear, which ultimately results on the loss of the cutting edge.

The rake face of the tool resultant from machining the high heat input samples is presented in Figure 4.19, where no signs of crater wear can be observed.

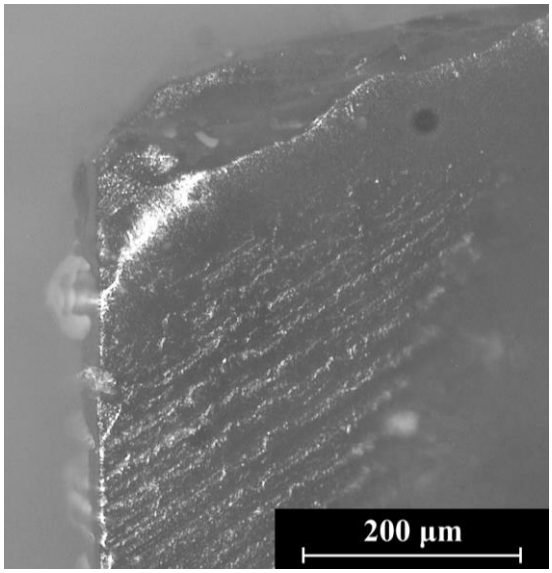

Figure 4.19 Rake face of the tool after machining experiment 12 on the high heat input samples

Polvorosa et al. [69] presented a study on the tool wear resultant from machining Inconel 718 and Waspalloy, observing the intensification of the adhesive mechanism on the tool rake face when machining the more ductile material. Hoier et al. [66] studied the influence of microstructural variations on the flank wear of 316 L austenitic steel, concluding that different metallurgical characteristics on similar materials from different fabricants can lead to distinct differences on the tool integrity.

Nevertheless, as mentioned before, with the increase of the distance from the substrate, the high heat input samples exhibited a higher dissimilarity on the grain size when compared with the low heat

input ones. Additionally, the high heat input specimens exhibited a higher elongation to fracture than those manufactured with a low heat input and the gradient of hardness is also higher on the high heat input samples. Knowing that a larger grain size eases the dislocation movement of the grains, the material would allow for more plastic deformation to occur, leading to larger chips that would increase the friction between the tool/chip interface, causing the abrasion mechanism to be more detrimental on the tool integrity. Furthermore, the higher hardness of the workpiece material also intensifies this wear mechanism, by increasing the resistance to shear.

With all these factors influencing the cutting process and with the applied experimental procedure, it is not possible to isolate their influence on the tool wear during machining. However, it is still noticeable that the abrasion and adhesion mechanisms had a significant impact on the tool integrity. Furthermore, another factor that might have had influence on different types of wear exhibited by the two types of samples, is the compressive residual stresses that the WAAM parts tend to exhibit with the increase of height [11,12]. These can hinder the cutting process and the tool integrity, by increasing the resistance to fracture of the workpiece material.

Moreover, the resultant tool integrity from both samples reflects the necessity for further investigation on the tool life within the different mechanical properties that the WAAM process can provide.

4.5 Chip observations

Macroscopically, the chips collected during the experiments exhibited different morphologies when varying the milling process parameters. Nevertheless, the most noticeable differences between the three regions in study occurred at in higher level for the feed per tooth. The chip thickness measurements are presented in Appendix F.

As it can be seen in Figure 4.20, comparing the chips resultant from the base and the top, it can be observed a tendency to increase in dimension and to achieve a higher curvature radius. This evidences the influence of the grain size on the relative motion of grain dislocations.

The smaller chips at the base are due to the smaller grain size that composes such region. These allow the material to be more resistant to the dislocation movement imposed by the compression of the tool on the workpiece. The plastic deformation on the chips causes the material to become more fragile, hence, the stress concentration results on chip breakage. At the top region of larger chips can be observed, the higher ductility and the ease for the dislocation movement that the workpiece material presents.

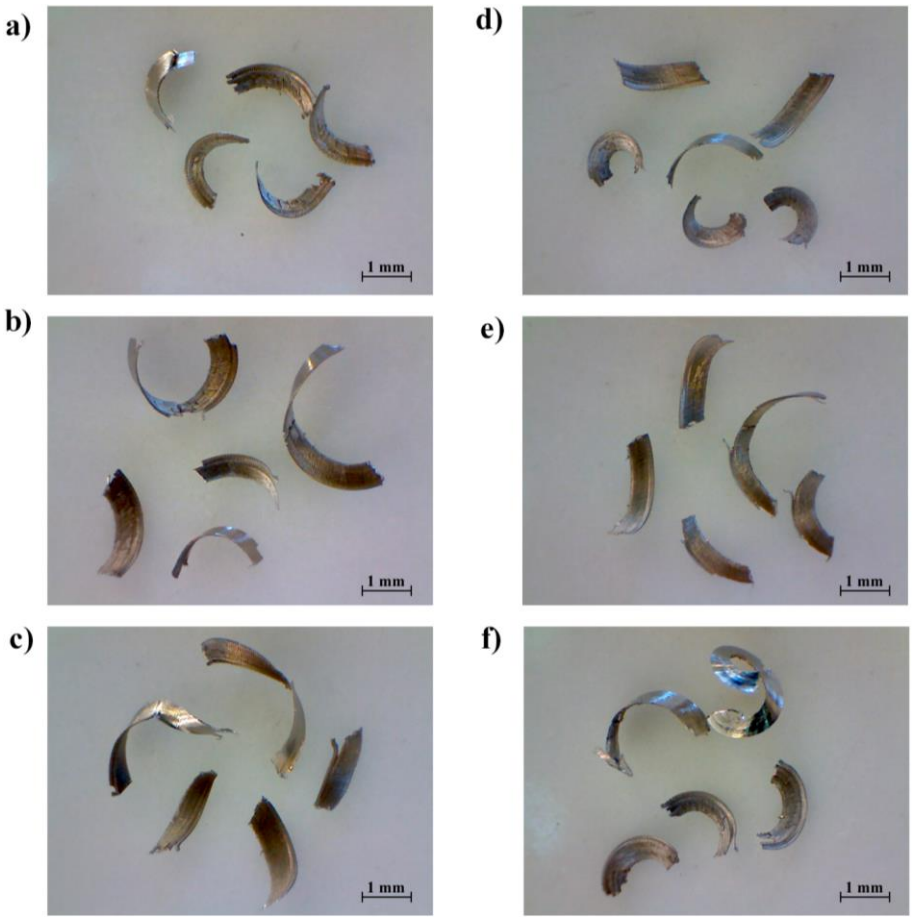

Figure 4.20 Different chip morphology between regions: Low heat input samples: a) Experiment 20, b) Experiment 22 and c) Experiment 24; High heat input samples: a) Experiment 20, b) Experiment 22 and c) Experiment 24

Additionally, it can also be observed that the chips resultant from the high heat input samples are longer and less fractured than those obtained on the low heat input case, especially the ones collected from the top region (see Figure 4.23 c) and f)).

4.5.1 Chip microscopy

The serrated morphology of the chips resultant form the milling experiments is presented in Figure 4.21. Here the primary and secondary shear zones can also be observed.

At the shear plane, where the uncut chip is being separated from the workpiece, the primary shear zone is resultant from the compressive forces exerted by the tool edge. Being inherently hard, the workpiece material resists to the movement of the tool and, when sufficiently high, these forces cause the workpiece material to fracture, developing serrations on the chips.

At the same time, the secondary shear zone is developed at the interface between the tool and the chip, where the friction on the surfaces causes the chips to be locally deformed.

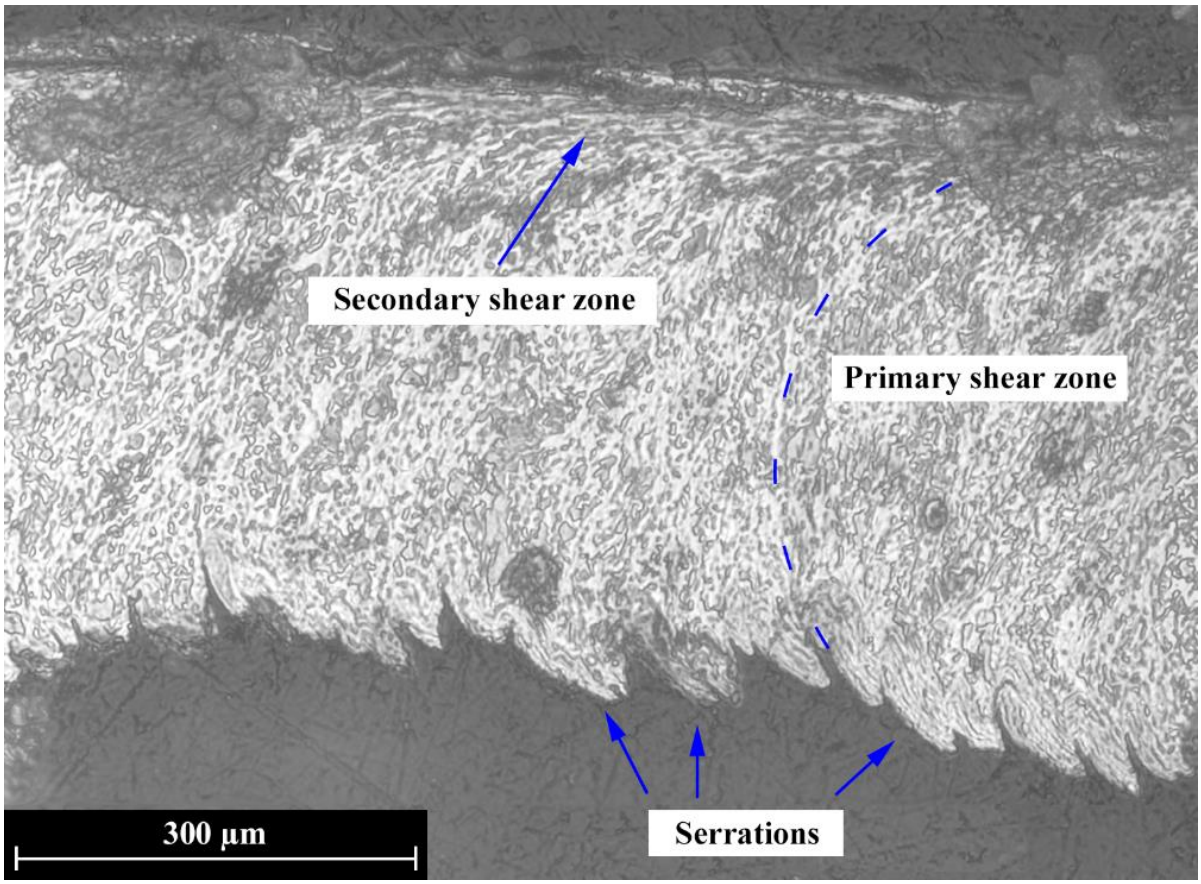

Figure 4.21 Chip resultant from experiment 19 of the low heat input samples

4.5.2 Results from the chip compression ratio

The chip compression ratio is a measure of the plastic deformation that occurs during the deformation of the chips that provides a correlation of the material properties with cutting performance.

Isolating the effect of the feed per tooth, which has the most influence on the chip thickness values, as it is given by Equation 2.1, in Figure 4.22 is presented a comparison of the chip compression ratio in terms of the cutting speed and machined region, for the feed per tooth value where the roughness measurements are less scattered (f_z=0.0115).

The discrepancy on the chip compression ratio when machining at low cutting speeds can be attributed to the formation of BUE, where the accumulation of material to the cutting edge, modifies the geometry of the tool, resulting on the non-linear variation of the thickness within a chip due to the adhesion of material to the chip.

At the centre, which is the region where the hardness is more uniform, it can be observed the increase on the chip compression ratio with the rise of cutting speed, which is attributed the thermal softening of the material caused by the increased friction between the tool/workpiece contact surfaces.

In the top region, the chip compression ratio is higher on the low heat input than in the high heat input samples. This can be attributed to the milling strategy, which started from the base towards the top, causing the cutting edge to be more deteriorated when machining such region, which resulted on a lower chip thickness.

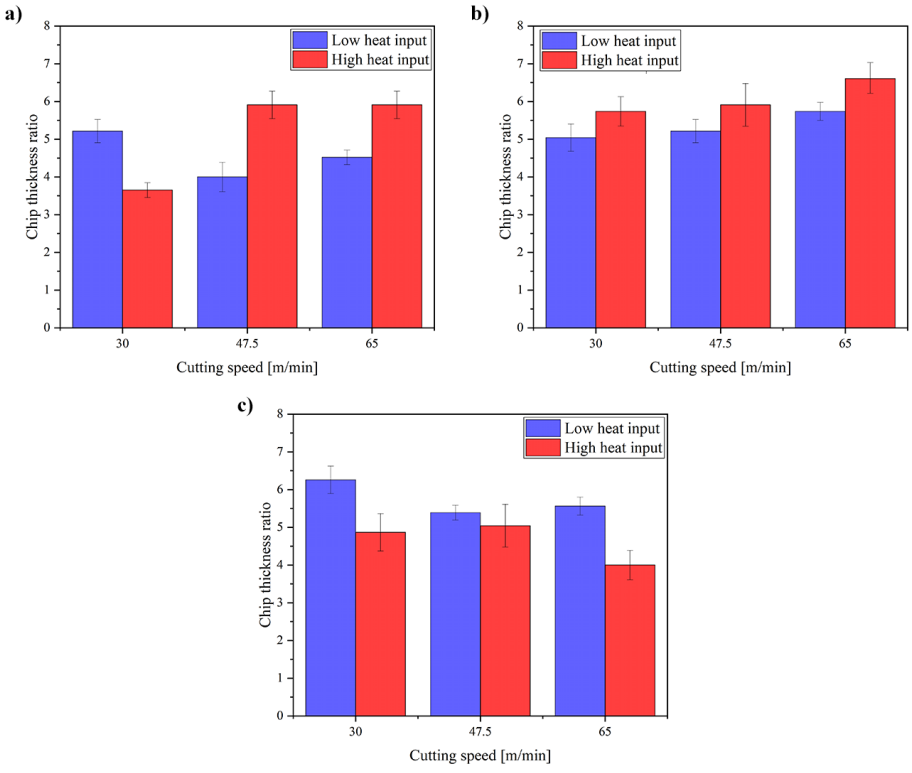

Figure 4.22 Chip compression ratio: a) Base; b) Centre; c) Top

4.6 Shear angle computation results

The computed values for the shear angle based on the measurement of the chips and on the cutting forces are presented in Figure 4.23 a) for the low heat input samples, and Figure 4.23 b) for the high heat input case. A tendency for the shear angle to increase can be observed in both figures, which can be attributed to the use of more severe parameters that ease the cutting process and to the tool state of wear developed during the process.

On the low heat input samples, the values diverge for the first set of experiments. This is due to the different approaches for the calculation of this angle, meaning that the force developed during the cut and the chip formation mechanisms may have behaved in a different form.

On the high heat input samples, however, the computed values are more scattered throughout the experiments, which can be due to the wear state of the tool and other factors caused to the different mechanical behaviour of these components.

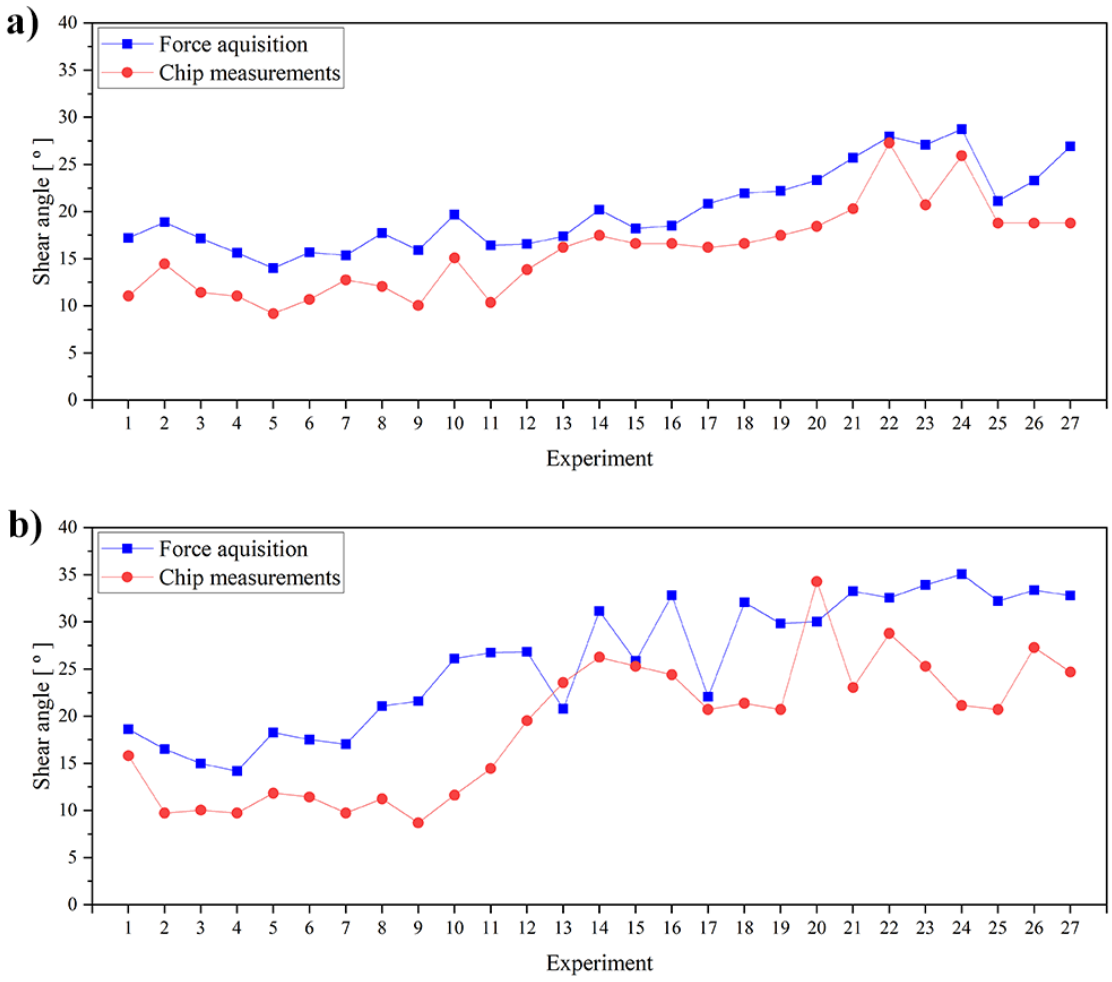

Figure 4.23 Computed shear angle: a) low heat input samples; b) high heat input samples

For both samples, the computed values based on the cutting forces are less dispersed than those obtained from the chips thickness measurements. However, being these results based on empirical models it may not provide the most accurate results for the case study of this thesis, provided that the several characteristics of the WAAM samples have influence on the cutting process. Additionally, the error associated with the measurement of the small chip thickness with an analogical micrometre, and with the cutting forces measurements renders the computed values to be only an approximation of the reality, provided that the tool integrity and the development of BUE also influences the cutting force measurements.

Some of the factors that may introduce uncertainty on the computed shear angle are:

- The formation of a build-up edge and/or a build-up layer, and the changes that it provides on the rake angle and tool geometry;
- The gradient on the mechanical properties that both samples exhibit, as a result of the WAAM process;
- The distribution and magnitude of the residual stresses in WAAM parts;
- The influence that the grain size causes in the chip removal process, evidenced by [67,68];

Additionally, other factors caused by the milling process also contribute to the propagation of error on the empirically obtained results. Such factors are:

- The runout provided by the geometrical differences between the teeth of each tool;
- The approximation of the uncut chip thickness provided by the classical view of the milling process.
- The degradation of the tool developed during machining, resultant from the actual chip removal process and the process parameters in use;
- The magnitude of the average cutting forces, utilized for the calculation of the specific cutting coefficients;
- The milling strategy utilized during the experiments, that isolates three regions, each with approximately similar mechanical behaviour, but that ignores the existence of punctual differences that might occur between the samples of the same type.

Therefore, different strategies for modelling the machining process outcomes are required to study more accurately the phenomena associated with the machining of WAAM parts. Additionally, the use of different cooling techniques to refrigerate and to ease the chip removal, should yield different results on the shear angle, cutting forces and on the chip formation mechanisms.

5

Conclusions and Future work

This thesis had the main objective to investigate the milling process on components produced with different heat inputs via Wire and arc additive manufacturing.

The literature regarding the WAAM process and the challenges that need to be surpassed in order to make it a viable technology for the industry, was reviewed. However, the current state-of-the-art reveals that, although several attempts have been made to study the post-processing of additive manufacturing parts, no researches focused on the cutting process of WAAM parts. Hence the need for applying known techniques for the characterization of the milling process on these components.

In a first stage of the experimental work, the thin-walled structures required for the milling operations were successfully manufactured and compared to those presented in the literature [10].

Secondly, a milling strategy that has in consideration the irregular mechanical properties distribution on the WAAM parts has been applied, in which the process parameters and the tools utilized during the experiments were chosen based on the information provided by the tool manufacturer, for machining different classes of steels.

Additionally, the mechanical properties inherent to HSLA steels, such as the excellent ductility and high yield strength, were found to have influence in the cutting process.

Based on the results the following conclusions can be drawn:

- For the low heat input samples, the surface roughness improved with the increase of the cutting speeds and with the decrease of the feed per tooth. The cutting forces, however, increase with the rise of the feed per tooth and with the decrease of cutting speeds. The worst surface roughness was achieved when machining with low cutting speeds.
- For the high heat input samples, similar trends to that of the low heat input samples, for the roughness and cutting forces were found. Still, the measurements were not totally accurate,

due to the tool condition, milling strategy and more pronounced gradient of the mechanical properties. The worst surface condition was found in experiment 12, although it is still admissible for roughing operations.

- Feed marks, pronounced grooves, material side flow and adhered material resultant from the formation of a build-up edge were observed on the machined surfaces.
- The cutting forces acquisition revealed the performance of the cut during the milling of a slot, where the decrease its magnitude with time, caused by the increase of the cutting temperatures, and the geometrical differences between the teeth were evidenced.
- The empirical approach utilized for accessing the shear angle revealed a similar cutting performance based on the cutting forces and on the chip measurements, for the low heat input samples.
- When exposed to the same milling strategy, the two types of samples behaved in a different manner in what concerns the tool wear. The adhesion and abrasion mechanisms were found to be responsible for the degradation of the cutting edges.
- Concerning the studied regions, the top of the high heat input samples presented the major challenges on the experimental results. Which can be attributed to the larger grain size that renders this region to produce longer and less fractured chips.
- Overall, the results from low heat input samples are indicators of the good performance of the milling process on the WAAM parts, although more investigation is required to study the cutting mechanism on the high heat input samples, due to tool wear. Hence, more resistant tools should be employed.
- Having into account the results, a different type of tool should be employed during the machining of this HSLA steel manufactured by WAAM, provided that the BUE formation and consequent deterioration of the tool were inevitable.
- On an industrial perspective, another possibility is to utilize a milling strategy that comprises different tools according to the machined regions, in order to isolate the influence of the WAAM characteristics, such as grain size and hardness, on the milling process.
- In comparison, the milling performance on the low heat input samples exhibited better results than the high heat input case, leading to the conclusion that it is important to consider the manufacturing method when executing post-processing operations on the WAAM components.

The future work required for the continuous development of the post-processing of WAAM parts through the cutting process relies on:

- The study on the tool wear mechanisms with different types of tools, maintaining the cutting parameters constant in the selected regions of both samples.

- Researching on a method for the simulation of tool wear, having in consideration the characteristics of the WAAM parts.
- Applying different milling strategies, sets of process parameters, types of tools and cooling strategies, in order to optimize the cutting procedure.
- Studying the formation of the build-up edge and burrs in the different regions through high speed imaging, in order to reduce their influence on the milling outcomes.
- Studying the milling process without removing the surface waviness characteristic of WAAM parts, in order to access the roughness profile and tool wear resultant from such operations.
- Studying the milling process on different materials produced with WAAM, where the ductility does not present a concern, such as titanium alloys.
- Studying the cutting process on components produced with different additive manufacturing techniques, in order to establish the differences between the manufacturing processes.

References

[1] J.M. Flynn, A. Shokrani, S.T. Newman, V. Dhokia, Hybrid additive and subtractive machine tools - Research and industrial developments, Int. J. Mach. Tools Manuf. 101 (2016) 79–101. doi:10.1016/j.ijmachtools.2015.11.007.

[2] T.D. Ngo, A. Kashani, G. Imbalzano, K.T.Q. Nguyen, D. Hui, Additive manufacturing (3D printing): A review of materials, methods, applications and challenges, Compos. Part B Eng. 143 (2018) 172–196. doi:10.1016/j.compositesb.2018.02.012.

[3] ISO, ASTM International, ISO/ASTM 52900:2015 -- Additive manufacturing — General principles — Terminology, ISOASTM 52900. (2015). doi:10.1520/ISOASTM52900-15.

[4] S.A.M. Tofail, E.P. Koumoulos, A. Bandyopadhyay, S. Bose, L. O'Donoghue, C. Charitidis, Additive manufacturing: scientific and technological challenges, market uptake and opportunities, Mater. Today. 21 (2018) 22–37. doi:10.1016/j.mattod.2017.07.001.

[5] C.R. Cunningham, J.M. Flynn, A. Shokrani, V. Dhokia, S.T. Newman, Invited review article: Strategies and processes for high quality wire arc additive manufacturing, Addit. Manuf. 22 (2018) 672–686. doi:10.1016/j.addma.2018.06.020.

[6] B. Wu, Z. Pan, D. Ding, D. Cuiuri, H. Li, J. Xu, J. Norrish, A review of the wire arc additive manufacturing of metals: properties, defects and quality improvement, J. Manuf. Process. 35 (2018) 127–139. doi:10.1016/j.jmapro.2018.08.001.

[7] T.A. Rodrigues, V. Duarte, R.M. Miranda, T.G. Santos, J.P. Oliveira, Current Status and Perspectives on Wire and Arc Additive Manufacturing (WAAM), Materials. 12 (2019) 1121. doi:10.3390/ma12071121.

[8] W. Zhang, A. De, A. Wilson-Heid, A.M. Beese, J.W. Elmer, J.S. Zuback, T. Mukherjee, J.O. Milewski, T. DebRoy, H.L. Wei, Additive manufacturing of metallic components – Process, structure and properties, Prog. Mater. Sci. 92 (2017) 112–224. doi:10.1016/j.pmatsci.2017.10.001.

[9] J. Xiong, Y. Li, R. Li, Z. Yin, Influences of process parameters on surface roughness of multi-layer single-pass thin-walled parts in GMAW-based additive manufacturing, J. Mater. Process. Technol. 252 (2018) 128–136. doi:10.1016/j.jmatprotec.2017.09.020.

[10] T.A. Rodrigues, V. Duarte, J.A. Avila, T.G. Santos, R.M. Miranda, J.P. Oliveira, Wire and arc additive manufacturing of HSLA steel: Effect of thermal cycles on microstructure and mechanical properties, Addit. Manuf. 27 (2019) 440–450. doi:10.1016/j.addma.2019.03.029.

[11] B.A. Szost, S. Terzi, F. Martina, D. Boisselier, A. Prytuliak, T. Pirling, M. Hofmann, D.J. Jarvis, A comparative study of additive manufacturing techniques: Residual stress and

microstructural analysis of CLAD and WAAM printed Ti–6Al–4V components, Mater. Des. 89 (2016) 559–567. doi:10.1016/j.matdes.2015.09.115.

[12] J.R. Hönnige, P.A. Colegrove, S. Ganguly, E. Eimer, S. Kabra, S. Williams, Control of residual stress and distortion in aluminium wire + arc additive manufacture with rolling, Addit. Manuf. 22 (2018) 775–783. doi:10.1016/j.addma.2018.06.015.

[13] P.A. Colegrove, H.E. Coules, J. Fairman, F. Martina, T. Kashoob, H. Mamash, L.D. Cozzolino, Microstructure and residual stress improvement in wire and arc additively manufactured parts through high-pressure rolling, J. Mater. Process. Technol. 213 (2013) 1782–1791. doi:10.1016/j.jmatprotec.2013.04.012.

[14] F. Martina, J. Ding, S. Williams, A. Caballero, G. Pardal, L. Quintino, Tandem metal inert gas process for high productivity wire arc additive manufacturing in stainless steel, Addit. Manuf. 25 (2019) 545–550. doi:10.1016/j.addma.2018.11.022.

[15] Y. Feng, B. Zhan, J. He, K. Wang, The double-wire feed and plasma arc additive manufacturing process for deposition in Cr-Ni stainless steel, J. Mater. Process. Technol. 259 (2018) 206–215. doi:10.1016/j.jmatprotec.2018.04.040.

[16] C. Shen, Z. Pan, Y. Ma, D. Cuiuri, H. Li, Fabrication of iron-rich Fe-Al intermetallics using the wire-arc additive manufacturing process, Addit. Manuf. 7 (2015) 20–26. doi:10.1016/j.addma.2015.06.001.

[17] A. Lopez, R. Bacelar, I. Pires, T.G. Santos, J.P. Sousa, L. Quintino, Non-destructive testing application of radiography and ultrasound for wire and arc additive manufacturing, Addit. Manuf. 21 (2018) 298–306. doi:10.1016/j.addma.2018.03.020.

[18] W. Du, Q. Bai, B. Zhang, Machining characteristics of 18Ni-300 steel in additive/subtractive hybrid manufacturing, Int. J. Adv. Manuf. Technol. 95 (2018) 2509–2519. doi:10.1007/s00170-017-1364-0.

[19] S. Sartori, L. Moro, A. Ghiotti, S. Bruschi, On the tool wear mechanisms in dry and cryogenic turning Additive Manufactured titanium alloys, Tribol. Int. 105 (2017) 264–273. doi:10.1016/j.triboint.2016.09.034.

[20] A. Bordin, S. Sartori, S. Bruschi, A. Ghiotti, Experimental investigation on the feasibility of dry and cryogenic machining as sustainable strategies when turning Ti6Al4V produced by Additive Manufacturing, J. Clean. Prod. 142 (2017) 4142–4151. doi:10.1016/j.jclepro.2016.09.209.

[21] T. Grove, B. Denkena, O. Maiß, A. Krödel, H. Schwab, U. Kühn, Cutting mechanism and surface integrity in milling of Ti-5553 processed by selective laser melting, J. Mech. Sci. Technol. 32 (2018) 4883–4892. doi:10.1007/s12206-018-0936-8.

[22] G. Struzikiewicz, W. Zębala, B. Słodki, Cutting parameters selection for sintered alloy AlSi10Mg longitudinal turning, Measurement. 138 (2019) 39–53. doi:10.1016/j.measurement.2019.01.082.

[23] A. Fortunato, A. Lulaj, S. Melkote, E. Liverani, A. Ascari, D. Umbrello, Milling of maraging steel components produced by selective laser melting, Int. J. Adv. Manuf. Technol. 94 (2018) 1895–1902. doi:10.1007/s00170-017-0922-9.

[24] G. Rotella, S. Imbrogno, S. Candamano, D. Umbrello, Surface integrity of machined additively manufactured Ti alloys, J. Mater. Process. Technol. 259 (2018) 180–185. doi:10.1016/j.jmatprotec.2018.04.030.

[25] O. Oyelola, P. Crawforth, R. M'Saoubi, A.T. Clare, On the machinability of directed energy deposited Ti6Al4V, Addit. Manuf. 19 (2018) 39–50. doi:10.1016/j.addma.2017.11.005.

[26] S. Bruschi, R. Bertolini, A. Bordin, F. Medea, A. Ghiotti, Influence of the machining parameters and cooling strategies on the wear behavior of wrought and additive manufactured Ti6Al4V for biomedical applications, Tribol. Int. 102 (2016) 133–142. doi:10.1016/j.triboint.2016.05.036.

[27] A. Calleja, G. Urbikain, H. González, I. Cerrillo, R. Polvorosa, A. Lamikiz, Inconel®718 superalloy machinability evaluation after laser cladding additive manufacturing process, Int. J. Adv. Manuf. Technol. 97 (2018) 2873–2885. doi:10.1007/s00170-018-2169-5.

[28] Y. Gong, P. Li, Analysis of tool wear performance and surface quality in post milling of additive manufactured 316L stainless steel, J. Mech. Sci. Technol. 33 (2019) 2387–2395. doi:10.1007/s12206-019-0237-x.

[29] Y. Bai, A. Chaudhari, H. Wang, Investigation on the microstructure and machinability of ASTM A131 steel manufactured by directed energy deposition, J. Mater. Process. Technol. (2019) 116410. doi:10.1016/j.jmatprotec.2019.116410.

[30] ADDITIVE MANUFACTURING Machines by DMG MORI, (n.d.). https://en.dmgmori.com/products/machines/additive-manufacturing (accessed September 13, 2019).

[31] Hybrid Multi-Tasking Machine | Mazak EU, (n.d.). https://www.mazakeu.com/machines-technology/technology/hybrid-multi-tasking-machine/ (accessed September 13, 2019).

[32] Hybrid Manufacturing: Additive or Subtractive, Https://Dmscncrouters.Com/. (n.d.). https://dmscncrouters.com/hybrid-manufacturing/ (accessed September 13, 2019).

[33] Hybrid Manufacturing Technologies, Hybrid Manuf. Technol. (n.d.). http://www.hybridmanutech.com/ (accessed September 13, 2019).

[34] Y. Shao, C. Liu, Z. Yan, H. Li, Y. Liu, Formation mechanism and control methods of acicular ferrite in HSLA steels: A review, J. Mater. Sci. Technol. 34 (2018) 737–744. doi:10.1016/j.jmst.2017.11.020.

[35] J. Hu, L.-X. Du, J.-J. Wang, Q.-Y. Sun, Cooling process and mechanical properties design of hot-rolled low carbon high strength microalloyed steel for automotive wheel usage, Mater. Des. 53 (2014) 332–337. doi:10.1016/j.matdes.2013.07.036.

[36] M. Talebi, M. Zeinoddini, M. Mo'tamedi, A.P. Zandi, Collapse of HSLA steel pipes under corrosion exposure and uniaxial inelastic cycling, J. Constr. Steel Res. 144 (2018) 253–269. doi:10.1016/j.jcsr.2018.02.003.

[37] S. Ragu Nathan, V. Balasubramanian, S. Malarvizhi, A.G. Rao, Effect of welding processes on mechanical and microstructural characteristics of high strength low alloy naval grade steel joints, Def. Technol. 11 (2015) 308–317. doi:10.1016/j.dt.2015.06.001.

[38] Q. Wang, S. Zhang, C. Zhang, J. Wang, M.B. Shahzad, H. Chen, J. Chen, A high strength low alloy steel fabricated by direct laser deposition, Vacuum. 161 (2019) 225–231. doi:10.1016/j.vacuum.2018.12.030.

[39] K.N. Shi, J.X. Ren, S.B. Wang, N. Liu, Z.M. Liu, D.H. Zhang, W.F. Lu, An improved cutting power-based model for evaluating total energy consumption in general end milling process, J. Clean. Prod. 231 (2019) 1330–1341. doi:10.1016/j.jclepro.2019.05.323.

[40] U. Karaguzel, E. Budak, Investigating effects of milling conditions on cutting temperatures through analytical and experimental methods, J. Mater. Process. Technol. 262 (2018) 532–540. doi:10.1016/j.jmatprotec.2018.07.024.

[41] H.Z. Li, K. Liu, X.P. Li, A new method for determining the undeformed chip thickness in milling, J. Mater. Process. Technol. 113 (2001) 378–384. doi:10.1016/S0924-0136(01)00586-6.

[42] G. Song, J. Li, J. Sun, Approach for modeling accurate undeformed chip thickness in milling operation, Int. J. Adv. Manuf. Technol. 68 (2013) 1429–1439. doi:10.1007/s00170-013-4932-y.

[43] L.M. Kumanchik, T.L. Schmitz, Improved analytical chip thickness model for milling, Precis. Eng. 31 (2007) 317–324. doi:10.1016/j.precisioneng.2006.12.001.

[44] M.E. Martellotti, An analysis of the milling process, Trans ASME. 63 (1941) 677.

[45] Z. Chang, Z.C. Chen, R. Mo, D. Zhang, Q. Deng, An accurate and efficient approach to geometric modeling of undeformed chips in five-axis CNC milling, Comput.-Aided Des. 88 (2017) 42–59. doi:10.1016/j.cad.2017.03.003.

[46] S. Lotfi, B. Rami, B. Maher, D. Gilles, B. Wassila, Cutter-workpiece engagement calculation in 3-axis ball end milling considering cutter runout, J. Manuf. Process. 41 (2019) 74–82. doi:10.1016/j.jmapro.2019.03.025.

[47] L. Sai, R. Belguith, M. Baili, G. Dessein, W. Bouzid, An approach to modeling the chip thickness and cutter workpiece engagement region in 3 and 5 axis ball end milling, J. Manuf. Process. 34 (2018) 7–17. doi:10.1016/j.jmapro.2018.05.018.

[48] J.J. Pamies Teixeira, Fundamentos Físicos do Corte dos Metais, Universidade Nova de Lisboa, 2001.

[49] Y. Altintas, Manufacturing automation: metal cutting mechanics, machine tool vibrations, and CNC design, Cambridge Univ. Press, Cambridge, 2000.

[50] V. Sivaraman, S. Sankaran, L. Vijayaraghavan, A study on the influence of cutting parameters on forces during machining the multiphase V-microalloyed steel, Int. J. Adv. Manuf. Technol. 79 (2015) 1285–1292. doi:10.1007/s00170-015-6921-9.

[51] Y.S. Ahmed, J.M. Paiva, B. Bose, S.C. Veldhuis, New observations on built-up edge structures for improving machining performance during the cutting of superduplex stainless steel, Tribol. Int. 137 (2019) 212–227. doi:10.1016/j.triboint.2019.04.039.

[52] I. Martinez, R. Tanaka, Y. Yamane, K. Sekiya, K. Yamada, T. Ishihara, S. Furuya, Wear mechanism of coated tools in the turning of ductile cast iron having wide range of tensile strength, Precis. Eng. 47 (2017) 46–53. doi:10.1016/j.precisioneng.2016.07.003.

[53] E.A. Rahim, H. Sasahara, A study of the effect of palm oil as MQL lubricant on high speed drilling of titanium alloys, Tribol. Int. 44 (2011) 309–317. doi:10.1016/j.triboint.2010.10.032.

[54] J. Kümmel, J. Gibmeier, E. Müller, R. Schneider, V. Schulze, A. Wanner, Detailed analysis of microstructure of intentionally formed built-up edges for improving wear behaviour in dry metal cutting process of steel, Wear. 311 (2014) 21–30. doi:10.1016/j.wear.2013.12.012.

[55] P. Sahoo, Surface topography, in: Tribol. Eng., Elsevier, 2011: pp. 1–32. doi:10.1533/9780857091444.1.

[56] A. Townsend, N. Senin, L. Blunt, R.K. Leach, J.S. Taylor, Surface texture metrology for metal additive manufacturing: a review, Precis. Eng. 46 (2016) 34–47. doi:10.1016/j.precisioneng.2016.06.001.

[57] ISO 4287, Geometrical Product Specifications (GPS) – Surface texture: Profile method – Terms, definitions and surface texture parameters, Int. Organ. Stand. (1997).

[58] DRATEC, DRATEC Drahttechnik GmbH, (n.d.).

[59] H. Geng, J. Li, J. Xiong, X. Lin, D. Huang, F. Zhang, Formation and improvement of surface waviness for additive manufacturing 5A06 aluminium alloy component with GTAW system, Rapid Prototyp. J. 24 (2018) 00–00. doi:10.1108/RPJ-04-2016-0064.

[60] DORMER Pramet, DORMER Catalogue, (2018).

[61] D. ISO 4288, Geometrical Product Specifications (GPS)-Surface texture: Profile method-Rules and procedures for the assessment of surface texture, Switzerland, 1996.

[62] ISO, 8688-2:1989 Tool Life Testing in Milling, Part II- End Milling, (1989).

[63] L.K. Gillespie, P.T. Blotter, The Formation and Properties of Machining Burrs, J. Eng. Ind. 98 (1976) 66. doi:10.1115/1.3438875.

[64] S.A. Niknam, Modeling and experimental characterization of the friction effects on orthogonal milling exit burrs, Int. J. Adv. Manuf. Technol. 91 (2017) 1079–1089. doi:10.1007/s00170-016-9828-1.

[65] Y. Houchuan, C. Zhitong, Z. ZiTong, Influence of cutting speed and tool wear on the surface integrity of the titanium alloy Ti-1023 during milling, Int. J. Adv. Manuf. Technol. 78 (2015) 1113–1126. doi:10.1007/s00170-014-6593-x.

[66] P. Hoier, A. Malakizadi, S. Friebe, U. Klement, P. Krajnik, Microstructural variations in 316L austenitic stainless steel and their influence on tool wear in machining, Wear. 428–429 (2019) 315–327. doi:10.1016/j.wear.2019.02.024.

[67] S. Olovsjö, L. Nyborg, Influence of microstructure on wear behaviour of uncoated WC tools in turning of Alloy 718 and Waspaloy, Wear. 282–283 (2012) 12–21. doi:10.1016/j.wear.2012.01.004.

[68] S. Olovsjö, A. Wretland, G. Sjöberg, The effect of grain size and hardness of Waspaloy on the wear of cemented carbide tools, Int. J. Adv. Manuf. Technol. 50 (2010) 907–915. doi:10.1007/s00170-010-2590-x.

[69] R. Polvorosa, A. Suárez, L.N.L. de Lacalle, I. Cerrillo, A. Wretland, F. Veiga, Tool wear on nickel alloys with different coolant pressures: Comparison of Alloy 718 and Waspaloy, J. Manuf. Process. 26 (2017) 44–56. doi:10.1016/j.jmapro.2017.01.012.

Appendix A – Technical drawing of the fixture

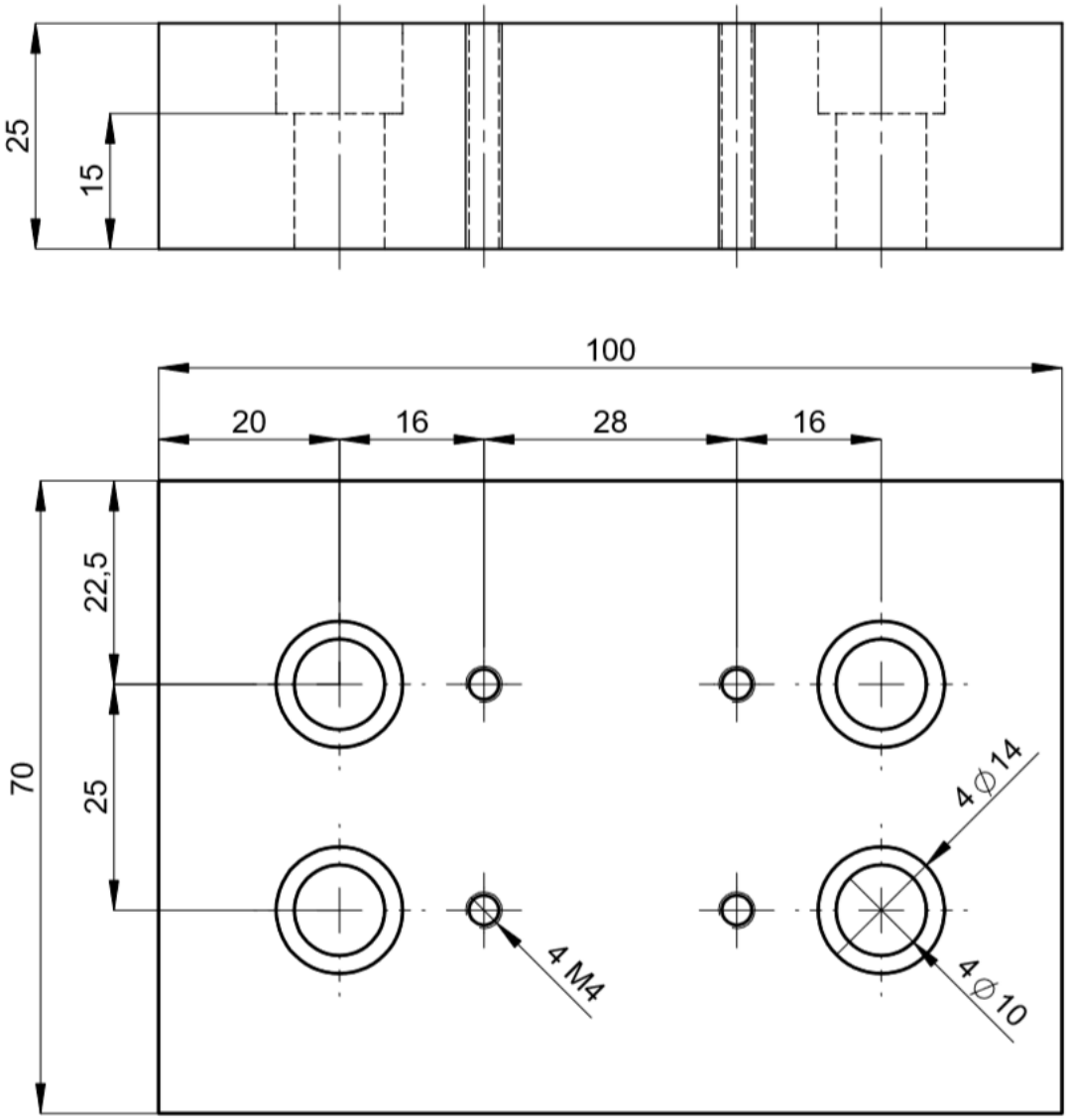

Dimensions in millimetres
Not to scale

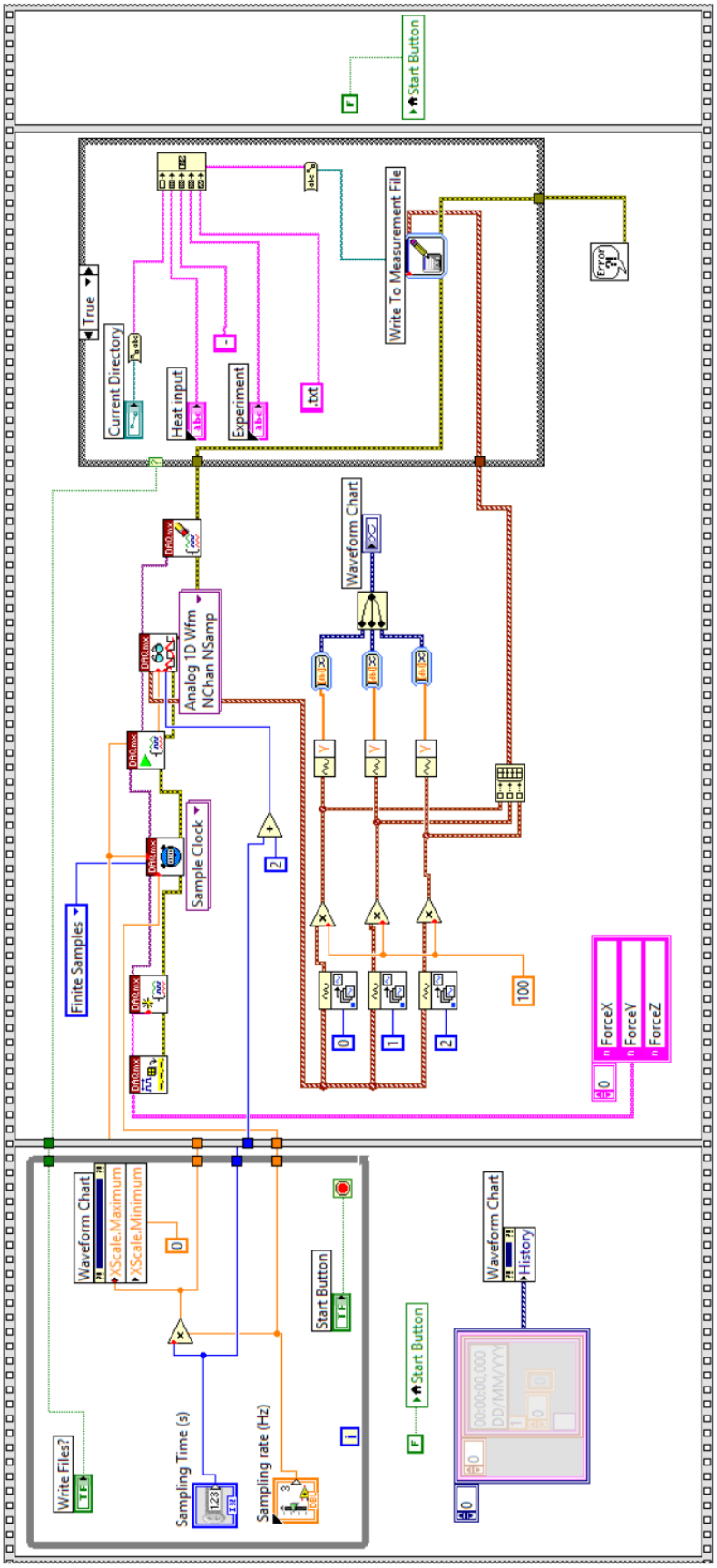
Start Button
True
Current Directory
Heat input
Experiment
.txt
Write To Measurement File
Error out
Waveform Chart
Analog 1D Wfm NChan NSamp
Sample Clock
Finite Samples
2
100
ForceX
ForceY
ForceZ
0
1
2
Waveform Chart
XScale.Maximum
XScale.Minimum
Start Button
Write Files?
Sampling Time (s)
Sampling rate (Hz)
Waveform Chart
History
Start Button

Appendix D – Roughness measurements

Experiment	Low heat input				High heat input			
	Ra [µm] µ ± σ		Rz [µm] µ ±σ		Ra [µm] µ ± σ		Rz [µm] µ ± σ	
# 1	0.327	± 0.040	2.415	± 0.413	0.242	± 0.036	1.296	± 0.180
# 2	0.167	± 0.025	0.987	± 0.127	0.272	± 0.043	1.349	± 0.138
# 3	0.476	± 0.082	2.992	± 0.268	0.372	± 0.076	1.941	± 0.463
# 4	0.271	± 0.065	1.261	± 0.777	0.254	± 0.084	1.366	± 0.269
# 5	0.259	± 0.056	1.821	± 0.307	0.716	± 0.086	3.556	± 0.397
# 6	0.141	± 0.032	0.925	± 0.220	0.518	± 0.110	2.817	± 0.493
# 7	0.125	± 0.028	0.851	± 0.152	0.125	± 0.024	0.765	± 0.119
# 8	0.318	± 0.039	1.465	± 0.380	0.205	± 0.107	1.279	± 0.635
# 9	0.178	± 0.027	1.125	± 0.127	0.152	± 0.045	0.941	± 0.227
# 10	0.460	± 0.077	1.686	± 0.163	0.330	± 0.094	1.773	± 0.489
# 11	0.131	± 0.031	0.870	± 0.108	0.262	± 0.086	1.443	± 0.469
# 12	0.346	± 0.019	1.158	± 0.146	0.638	± 0.104	3.300	± 0.451
# 13	0.211	± 0.053	1.212	± 0.219	0.377	± 0.045	2.138	± 0.230
# 14	0.168	± 0.060	1.350	± 0.190	0.131	± 0.031	0.978	± 0.205
# 15	0.326	± 0.081	1.955	± 0.356	0.243	± 0.050	1.305	± 0.218
# 16	0.214	± 0.088	1.558	± 0.557	0.259	± 0.088	1.223	± 0.337
# 17	0.202	± 0.014	0.896	± 0.040	0.210	± 0.034	1.115	± 0.199
# 18	0.144	± 0.037	1.134	± 0.367	0.216	± 0.020	1.231	± 0.149
# 19	0.390	± 0.028	2.113	± 0.269	0.496	± 0.016	2.497	± 0.107
# 20	0.208	± 0.080	1.088	± 0.423	0.404	± 0.030	2.035	± 0.204
# 21	0.584	± 0.023	3.116	± 0.162	0.653	± 0.082	3.184	± 0.355
# 22	0.361	± 0.066	1.261	± 0.186	0.658	± 0.038	2.791	± 0.178
# 23	0.146	± 0.097	2.664	± 0.465	0.551	± 0.090	2.557	± 0.307
# 24	0.280	± 0.025	1.516	± 0.101	0.513	± 0.056	2.377	± 0.319
# 25	0.238	± 0.040	1.117	± 0.333	0.189	± 0.010	1.159	± 0.193
# 26	0.231	± 0.057	1.289	± 0.207	0.213	± 0.035	1.226	± 0.149
# 27	0.154	± 0.025	0.893	± 0.171	0.245	± 0.029	1.256	± 0.255

Appendix E – Maximum cutting force measurements

Experiment	Low heat input			High heat input		
	Resultant cutting force [N] μ ±σ			Resultant cutting force [N] μ ±σ		
# 1	62.691	±	5.372	52.151	±	2.787
# 2	55.625	±	4.450	57.148	±	3.120
# 3	68.861	±	4.400	56.904	±	4.794
# 4	62.972	±	4.408	58.693	±	1.347
# 5	80.425	±	3.925	52.961	±	6.750
# 6	72.754	±	5.093	41.486	±	3.926
# 7	54.114	±	3.247	66.173	±	5.290
# 8	84.383	±	3.131	115.963	±	8.949
# 9	56.913	±	3.984	81.532	±	2.722
# 10	85.034	±	4.201	120.512	±	6.563
# 11	61.871	±	3.094	103.657	±	4.544
# 12	90.898	±	5.045	151.254	±	24.252
# 13	74.704	±	4.482	63.704	±	2.903
# 14	58.304	±	4.347	46.668	±	2.496
# 15	74.630	±	5.224	60.750	±	2.940
# 16	63.466	±	4.812	45.317	±	2.025
# 17	82.365	±	6.589	60.956	±	1.111
# 18	65.240	±	7.829	48.798	±	1.053
# 19	78.784	±	4.367	74.698	±	5.187
# 20	68.668	±	4.120	68.354	±	3.160
# 21	83.227	±	4.161	87.285	±	1.342
# 22	82.921	±	4.146	78.415	±	1.934
# 23	98.807	±	4.940	97.365	±	7.427
# 24	92.008	±	6.441	112.395	±	2.322
# 25	89.026	±	3.561	65.365	±	1.148
# 26	82.369	±	3.295	72.951	±	3.190
# 27	64.227	±	3.561	64.482	±	1.948

Appendix F – Chip thickness measurements

Experiment	Low heat input samples			High heat input samples		
	μ ± σ			μ ± σ		
# 1	0.060	±	0.007	0.042	±	0.004
# 2	0.046	±	0.009	0.068	±	0.008
# 3	0.058	±	0.008	0.066	±	0.009
# 4	0.060	±	0.007	0.068	±	0.013
# 5	0.072	±	0.008	0.056	±	0.011
# 6	0.062	±	0.004	0.058	±	0.013
# 7	0.052	±	0.004	0.068	±	0.008
# 8	0.110	±	0.020	0.118	±	0.013
# 9	0.066	±	0.005	0.076	±	0.009
# 10	0.088	±	0.004	0.114	±	0.017
# 11	0.064	±	0.005	0.046	±	0.009
# 12	0.096	±	0.019	0.068	±	0.008
# 13	0.082	±	0.011	0.056	±	0.005
# 14	0.076	±	0.005	0.050	±	0.010
# 15	0.080	±	0.014	0.052	±	0.008
# 16	0.080	±	0.010	0.054	±	0.011
# 17	0.082	±	0.008	0.064	±	0.009
# 18	0.080	±	0.016	0.062	±	0.013
# 19	0.114	±	0.018	0.096	±	0.011
# 20	0.108	±	0.016	0.056	±	0.009
# 21	0.098	±	0.019	0.086	±	0.011
# 22	0.072	±	0.004	0.068	±	0.013
# 23	0.096	±	0.005	0.078	±	0.008
# 24	0.076	±	0.005	0.094	±	0.015
# 25	0.106	±	0.009	0.096	±	0.009
# 26	0.106	±	0.011	0.072	±	0.011
# 27	0.106	±	0.005	0.080	±	0.007